# Title: Protein assemblies ejected directly from native membranes yield complexes for mass spectrometry

**Authors: Dror S. Chorev[1], Lindsay A. Baker[2], Di Wu[1], Victoria Beilsten-Edmands[1], Sarah L. Rouse[3], Tzviya Zeev-Ben-Mordehai[2,#], Chimari Jiko[4], Firdaus Samsudin[5], Christoph Gerle[6,7], Syma Khalid[5], Alastair G. Stewart[8,9], Stephen J. Matthews[3], Kay Grünewald[2,10], and Carol V. Robinson[1,*].**

**Affiliations:**

[1]Physical and Theoretical Chemistry Laboratory, South Parks Road, OX1 3QZ, University of Oxford, Oxford, UK.

[2]Division of Structural Biology, Roosevelt drive, OX3 7BN, University of Oxford, Oxford, UK.

[3]Department of Life Sciences, Imperial College, London, South Kensington Campus, SW7 2AZ, UK.

[4]Institute for Integrated Radiation and Nuclear Science, Kyoto University, Kumatori, Japan.

[5]School of Chemistry, University of Southampton, University Road, Southampton, SO17 1BJ, UK.

[6]Institute for Protein Research, Osaka University, Suita, Osaka, Japan.

[7]Core Research for Evolutional Science and Technology, Japan and Science and Technology Agency, Kawaguchi, Japan.

[8]Molecular, Structural and Computational Biology Division, Victor Chang Cardia Research Institute, Darlinghurst, Australia.

[9]Faculty of Medicine, The University of New South Wales, Sydney, Australia.

[10]Centre of Structural Systems Biology (CSSB), Notkestr. 85, D-22607, Heinrich-Pette Institute/ University of Hamburg, Hamburg, Germany.

[#]Current address: Cryo Electron Microscopy, Bijvoet Center for Biomolecular Research, Utrecht University, Utrecht 3584 CH, The Netherlands.

[*]Corresponding author:

Prof. Carol V. Robinson Carol.robinson@chem.ox.ac.uk

**Abstract:** Membrane proteins reside in lipid bilayers and are typically extracted from this environment for study, which often compromises their integrity. Here we eject intact assemblies from membranes, without chemical disruption, and use mass spectrometry to define their composition. From *E. coli* outer membranes, we identify a chaperone-porin association and lipid interactions in the beta-barrel assembly machinery. Bridging inner and outer membranes we observe efflux pumps, and from inner membranes a pentameric pore of TonB, and the protein-conducting channel Sec YEG, in association with $F_1F_O$ ATP-synthase. Intact mitochondrial membranes from *Bos taurus* yield respiratory complexes and fatty acid-bound dimers of the ADP/ATP transporter (ANT-1). These results highlight the importance of native membrane environments for retaining small-molecule binding, subunit interactions and associated chaperones of the membrane proteome.

**One Sentence Summary:** Mass spectra reveal the composition of complexes ejected directly from native membrane environments.

**Main Text:** Genes encoding membrane proteins comprise between 20-30% of the genome of all living cells and perform critical processes ranging from mediating drug resistance in bacteria through to the complex mitochondrial respiratory chain in humans. Recent developments in structural biology, including high-resolution cryo-electron microscopy (EM), are uncovering new structures and roles of membrane proteins (*1*). Often, subunit stoichiometry and lipid binding properties of complexes extracted in detergent micelles has been controversial prompting development of native mass spectrometry (nMS) methods. Now broadly accepted for retaining the stoichiometry of soluble complexes (*2*) recent developments in nMS of membrane proteins assemblies have not only uncovered subunit stoichiometries but have also found roles for lipids in modulating structures (*3, 4*). To reveal stoichiometry and lipid binding in the absence of detergents alternative nMS approaches have been developed, including bicelles (*5*), amphipols (*6*), nanodiscs (*7*), and styrene maleic acid copolymer lipid particles (SMALPs) (*8*). All these approaches require some chemical intervention and high levels of protein expression, thereby restricting their use primarily to proteins of bacterial origin. Here we overcome these

limitations and show that we can obtain mass spectra for protein assemblies ejected directly from native membranes of prokaryotic and eukaryotic organisms and uncover many previously uncharacterized interactions in the process.

To develop this approach we first used membrane protein enriched extracellular vesicles (MPEEVs) overexpressing the Epithelial Fusion Failure protein 1 (EFF-1), reported to be monomeric, or the Anchor Cell Fusion Failure protein 1 (AFF-1) with unknown stoichiometry (*9, 10*). MPEEVs of both proteins from Syrian hamster BHK21 cultured cells were prepared and characterised as described previously (*9*). The presence of either EFF-1 or AFF-1 increased the diversity of cardiolipins (CDL) as was confirmed by standard approaches (fig. S1A and C). Subjecting these vesicles to sonication, to destabilize their integrity (see Online Methods and fig. S2), and to high energy across a modified Orbitrap MS (*11*), we released monomeric EFF-1 and intact dimeric AFF-1 directly from vesicles (fig. S1B).

Having established the feasibility of our approach, we investigated its application to additional native membranes. We separated outer and inner membranes of *E. coli* via a sucrose gradient, prepared vesicles and used proteomics to identify membrane proteins (*12*) (fig. S3). To interpret the mass spectra we developed and applied a protocol that takes into account peak width, collision induced dissociation (CID) and accurate mass only accepting solutions within ± ~ 0.3 % of calculated masses (fig. S2 and Tables S1-3). Starting from the low m/z range of the spectrum recorded for *E. coli* outer membranes we assigned BamC with a lipid anchor, a component of the beta barrel assembly machinery (BAM) (fig. 1A) (*13*). Moving to higher m/z we assign DnaK, implicated previously in the assembly of outer membrane porins (*14*) and confirmed via CID of a 143 kDa complex together with OmpA (fig. S4). Previous reports that DnaK co-immunoprecipitates with full-length pro-OmpA, but not with pro-OmpA(Δ3) (*14*), implied that sequences outside the β-barrel are required to maintain accessibility of DnaK binding sites. Our measured mass (within 0.10 %) is consistent with ADP-bound DnaK binding to proOmpA and associating with a second OmpA, likely through the C-terminal dimerisation domain (*15*), to form OmpA:proOmpA:DnaK:ADP (fig. 1B).

Turning to the high m/z region of the mass spectrum recorded for outer membranes, a predominant series of peaks was assigned to BAM (*13*). Structural studies, following detergent

extraction and overexpression of all five subunits on a single plasmid yielded primarily a 1:1:1:1:1 stoichiometry for Bam subunits (A-E) (*13, 16, 17*). From native membranes however, a hexamer was ejected with a subunit composition of $ABCD(E)_2$ (fig. 1A and D), a small population of this complex had been observed previously from recombinant preparations (*17*). Since a domain swapped dimer was observed by x-ray analysis of Bam E alone (*18*), and NMR solution studies were consistent with a population of BamE dimers (*19*), we docked into Bam ABCD a BamE dimer and used MD simulation to test its stability (*20*). The complex remained stable over 5 μs, following heating to 323 K, consistent with its viability in the *E. coli* outer membrane lipid environment. A second series was assigned to pentameric Bam ABCDE complex, its diffuse peaks consistent with binding of up to three CDL molecules (fig. 1C and fig. S5). Preferential binding of phosphatidylglycerol (PG) over CDL had been reported previously (*19*) prompting us to explore lipid binding preferences of BamE using MD simulations (3 x 5 μs) (fig. 1E and fig. S6). Up to three CDL lipids made contact implying CDL attachment, through BamE, which likely anchors the complex to a region of the membrane high in CDL and may contribute to a membrane targeting mechanism.

Inner membrane vesicles prepared from *E. coli* represent a significant challenge as together they contain a minimum of 42 different proteins (*12*) and yield complex spectra for assignment (fig. S7). We used the heterogeneity of cofactor binding to first identify cytochromes $bo_3$ and CydAB bd oxidase. Peaks corresponding to $(CyoB)_2(CyoC)_1(CyoD)_1$, with one or two $HemeO_3$/HemeB factors and additional CDL binding (diffuse peaks) imply that lipid binding stabilizes structures with the full-heme complement, supported by reduced charge state (fig. 2A) and in-line with the proposed dimer association for cytochrome $bo_3$ from native membranes (*21*). Extensive peak splitting attributed to different Heme groups (B558, B595) and ubiquinol helped identify the CydAB cytochrome bd oxidase complex (fig. 2B and fig. S8). Both CydX and the paralogous small transmembrane protein AppX have the potential to interact with the CydAB complex and have overlapping cellular functions (*22*). From the native membrane we found that CydX and AppX were able to interact simultaneously with CydAB to form a heterotetramer.

We next assigned, on the basis of mass, parts of the energy-transducing Ton complex located within the inner membrane. In the inner membrane three integral membrane proteins reside:

ExbB, ExbD and TonB. From x-ray crystallography a second copy of ExbD was located within the pentameric ExbB pore (*23*) while from EM both hexameric and pentameric assemblies were defined (*24*). Our results confirm the existence of only the pentameric pore within the native membrane with measured charge states implying trapping of one ExbD protomer within the compact globular complex (fig. 2B).

At the higher m/z region sub-assemblies of multidrug efflux pumps, including AcrAB-TolC and the less well-characterised but related pump MdtABTolC (*25*), were uncovered spanning both membranes (fig. 2C). For AcrAB-TolC all three inner membrane subunits (AcrB) are preserved in mass spectra bound to the small subunit (AcrZ) discovered only recently, thought to modulate substrate preference (*26*) and modelled into cryo-EM structures (*27*). One copy of the outer membrane protein TolC is bridged by a single copy of the periplasmic subunit AcrA to the inner membrane complex yielding $AcrB_3$:$AcrZ_2$:AcrA:TolC. In the case of MdtABTolC dimeric MdtB remains assembled with $(MdtA)_3$ and $(TolC)_2$ in the outer membrane ($MdtB_2MdtA_3$:$TolC_2$). Since all three MdtA subunits remain attached they are likely supported by dimeric MdtB in the inner membrane, consistent with the role of MdtC in substrate binding (*28*) and not in supporting periplasmic subunits. AcrABZ-TolC has undergone more extensive disassembly during the solution /sonication process than MdtAB-TolC which remains largely intact with charge states (fig. S9) indicative of highly-charged subunits from AcrABZ-TolC undergoing CID (*29*). The fact that both complexes survive at least in part, however, points to new ways of studying the effects of antibiotics on the assembly and conformational change of these multidrug resistance pumps.

We also observed peak splitting due to ATP/ADP binding, at the highest m/z values which, together with dissociation of subunits with the mass of the c-subunit, is indicative of ATP synthase (fig. 2C, figs. S10 and S11). Mass differences between populations were assigned to binding of SecE, Y and G, consistent with SecYEG remaining in contact with the $F_1F_O$ATP synthase as reported previously for insertion of subunit *a* (*30*). We next considered the stoichiometry of the $F_O$ ring. Early reports had suggested a variable stoichiometry depending upon metabolic conditions (*31*), our data are consistent with 12 c subunits in the $F_O$ ring. We conclude therefore that in the native membrane interactions between $F_OF_1$ ATPase and SecYEG

are maintained following insertion in the membrane, together with c-subunits in $F_{O,}$ which are either lost during detergent extraction (*32*) or filtered out in other methods.

Observation of *E. coli* ATPase prompted us to consider inner mitochondrial membranes, densely populated with protein complexes responsible for control of the proton gradient and oxidative phosphorylation between the intermembrane space and the inner mitochondrial matrix (*33*). Surprisingly inner mitochondrial membranes from *Bos taurus* yielded only a single subunit of the ATPase (β) and no significant subassemblies of complex I (fig. 3A). Other complexes in the respiratory chain that were observed include complex II, monomeric complex IV with lipid and cofactor occupancy (*34*) and dimeric complex III, with seven core subunits confirmed by dissociation of cytochrome b and UQCRB (fig. 3A and fig. S12).

Interestingly the most abundant protein in the mass spectrum of the inner mitochondrial membrane was the adenine nucleotide translocase 1 (ANT-1) (fig. 3A). The stoichiometry of ANT-1 has remained controversial with monomeric structures of ANT-1 and UCP2 solved by X-ray crystallography and NMR, and proposed to be functional (*35-37*). However, *in-vivo* and biochemical experiments were consistent with the functional unit of ANTs and UCPs being dimeric (*38*), a proposal supported by short timescale by MD simulations (*39*). MS of ANT-1 revealed that it is predominantly dimeric with low occupancy binding of a number of saturated fatty acids (palmitate anions) indicative of a transport mechanism rather than specific binding interaction (fig. 3A and S13). MD simulations in lipid bilayers showed that within 10 μs tightly bound dimers formed only if CDL was present in the inner leaflet of the membrane (fig. S14). Fatty acid binding was also observed with the palmitate head group buried between two helices in each subunit (Y132 and F177) (fig. 3B, S14D and movie S1). *In situ* binding of multiple palmitate anions within the dimer ejected from the native mitochondrial membrane provides direct evidence in support of the role of this fatty acid in the control of uncoupling through ANT-1 transport (*40*).

Since complexes I and V were largely absent from spectra of inner mitochondrial membranes we applied our protocol to intact mitochondria, without prior separation of inner and outer membranes, reasoning that the outer membrane and non-inverted protein orientation may protect complexes exposed during sonication. Resulting mass spectra again revealed ANT-1 dimers

bound to palmitate (fig. S13), but also in this case lipid bound sub-assemblies of Complex I bound to its FMN cofactor and lipids, a Complex IV dimer (fig. 3C and S15), together with intact Complex V bound to nucleotides.

The release of complexes I and V, only when protected by the outer membrane, prompts consideration of the mechanism of direct ejection from native membranes. The three steps to consider are (i) formation of vesicles (ii) sonication in ammonium acetate to disrupt vesicles and (iii) mass spectrometry under high electric fields from -400 to -700 V. During the first step vesicles are formed from membrane preparations with protein complexes in both orientations. For purified inner mitochondrial membranes, we observe primarily inside-out vesicles with ATPase $F_1$ heads visible in cryo-EM images (fig. S16). We anticipate that sonication may form defects in vesicles allowing ingress of the ammonium acetate buffer used for electrospray. The third stage, in which high voltage is applied, favors expulsion of complexes charged by the electrospray process and attracted by the high electric field. Striking differences are observed between the two preparations from mitochondria. For inner membranes we attribute the virtual absence of intact mitochondrial ATP synthase to exposure to shearing forces during sonication. Similar arguments could be made for the non-appearance of complex I from inner membranes; its exposed hydrophilic peripheral arm may have sheared during sonication leaving the hydrophobic membrane embedded complex less susceptible to charge. By contrast for intact mitochondria complexes I and V are ejected, largely intact, supporting the hypothesis that exposure to shearing forces during sonication is a key determinant in survival of complexes ejected from native membranes.

While full details of the mechanism of ejection from native membranes into vacuum are the subject of ongoing research the data presented here establish a detergent and chemical free MS approach that overcomes potential artefacts introduced by the use of these reagents. The number of new interactions of membrane proteins uncovered, with lipids, chaperones and cofactors in association, is testament to the stability endowed by the native membrane. Significantly, access to the protein ensemble of different membrane compartments, at unparalleled mass resolution, will enable a new perspective on the effects of drugs and disease associated mutations on target complexes within the context of their native membrane environments.

**References and Notes:**


1. K. R. Vinothkumar, R. Henderson, Single particle electron cryomicroscopy: trends, issues and future perspective. *Q Rev Biophys* **49**, e13 (2016).
2. A. J. Heck, Native mass spectrometry: a bridge between interactomics and structural biology. *Nat Methods* **5**, 927-933 (2008).
3. K. Gupta *et al.*, The role of interfacial lipids in stabilizing membrane protein oligomers. *Nature* **541**, 421-424 (2017).
4. A. Laganowsky *et al.*, Membrane proteins bind lipids selectively to modulate their structure and function. *Nature* **510**, 172-175 (2014).
5. J. T. Hopper *et al.*, Detergent-free mass spectrometry of membrane protein complexes. *Nat Methods* **10**, 1206-1208 (2013).
6. C. Bechara *et al.*, MALDI-TOF mass spectrometry analysis of amphipol-trapped membrane proteins. *Analytical chemistry* **84**, 6128-6135 (2012).
7. M. T. Marty, K. K. Hoi, J. Gault, C. V. Robinson, Probing the Lipid Annular Belt by Gas-Phase Dissociation of Membrane Proteins in Nanodiscs. *Angew Chem Int Ed Engl* **55**, 550-554 (2016).
8. V. Postis *et al.*, The use of SMALPs as a novel membrane protein scaffold for structure study by negative stain electron microscopy. *Biochim Biophys Acta* **1848**, 496-501 (2015).
9. T. Zeev-Ben-Mordehai, D. Vasishtan, C. A. Siebert, C. Whittle, K. Grunewald, Extracellular vesicles: a platform for the structure determination of membrane proteins by Cryo-EM. *Structure* **22**, 1687-1692 (2014).
10. T. Zeev-Ben-Mordehai, D. Vasishtan, C. A. Siebert, K. Grunewald, The full-length cell-cell fusogen EFF-1 is monomeric and upright on the membrane. *Nature communications* **5**, 3912 (2014).
11. M. van de Waterbeemd *et al.*, High-fidelity mass analysis unveils heterogeneity in intact ribosomal particles. *Nat Methods* **14**, 283-286 (2017).
12. F. Stenberg *et al.*, Protein complexes of the Escherichia coli cell envelope. *J Biol Chem* **280**, 34409-34419 (2005).
13. J. Bakelar, S. K. Buchanan, N. Noinaj, The structure of the beta-barrel assembly machinery complex. *Science* **351**, 180-186 (2016).
14. H. Y. Qi, J. B. Hyndman, H. D. Bernstein, DnaK promotes the selective export of outer membrane protein precursors in SecA-deficient Escherichia coli. *J Biol Chem* **277**, 51077-51083 (2002).
15. J. Marcoux *et al.*, Mass spectrometry defines the C-terminal dimerization domain and enables modeling of the structure of full-length OmpA. *Structure* **22**, 781-790 (2014).
16. Y. Gu *et al.*, Structural basis of outer membrane protein insertion by the BAM complex. *Nature* **531**, 64-69 (2016).
17. M. G. Iadanza *et al.*, Lateral opening in the intact β-barrel assembly machinery captured by cryo-EM. *Nature communications* **7**, 12865 (2016).
18. R. Albrecht, K. Zeth, Structural basis of outer membrane protein biogenesis in bacteria. *J Biol Chem* **286**, 27792-27803 (2011).
19. T. J. Knowles *et al.*, Structure and function of BamE within the outer membrane and the beta-barrel assembly machine. *EMBO Rep* **12**, 123-128 (2011).

20. P. C. Hsu, F. Samsudin, J. Shearer, S. Khalid, It Is Complicated: Curvature, Diffusion, and Lipid Sorting within the Two Membranes of Escherichia coli. *J Phys Chem Lett* **8**, 5513-5518 (2017).
21. F. Stenberg, G. von Heijne, D. O. Daley, Assembly of the cytochrome bo3 complex. *J Mol Biol* **371**, 765-773 (2007).
22. C. E. VanOrsdel *et al.*, The Escherichia coli CydX protein is a member of the CydAB cytochrome bd oxidase complex and is required for cytochrome bd oxidase activity. *J Bacteriol* **195**, 3640-3650 (2013).
23. H. Celia *et al.*, Structural insight into the role of the Ton complex in energy transduction. *Nature* **538**, 60-65 (2016).
24. S. Maki-Yonekura *et al.*, Hexameric and pentameric complexes of the ExbBD energizer in the Ton system. *Elife* **7**, (2018).
25. J. Anes, M. P. McCusker, S. Fanning, M. Martins, The ins and outs of RND efflux pumps in Escherichia coli. *Front Microbiol* **6**, 587 (2015).
26. E. C. Hobbs, X. Yin, B. J. Paul, J. L. Astarita, G. Storz, Conserved small protein associates with the multidrug efflux pump AcrB and differentially affects antibiotic resistance. *Proc Natl Acad Sci U S A* **109**, 16696-16701 (2012).
27. Z. Wang *et al.*, An allosteric transport mechanism for the AcrAB-TolC multidrug efflux pump. *Elife* **6**, (2017).
28. H. S. Kim, H. Nikaido, Different functions of MdtB and MdtC subunits in the heterotrimeric efflux transporter MdtB(2)C complex of Escherichia coli. *Biochemistry* **51**, 4188-4197 (2012).
29. Z. Hall, H. Hernandez, J. A. Marsh, S. A. Teichmann, C. V. Robinson, The role of salt bridges, charge density, and subunit flexibility in determining disassembly routes of protein complexes. *Structure* **21**, 1325-1337 (2013).
30. S. Kol *et al.*, Subunit a of the F(1)F(0) ATP synthase requires YidC and SecYEG for membrane insertion. *J Mol Biol* **390**, 893-901 (2009).
31. R. A. Schemidt, J. Qu, J. R. Williams, W. S. Brusilow, Effects of carbon source on expression of F0 genes and on the stoichiometry of the c subunit in the F1F0 ATPase of Escherichia coli. *J Bacteriol* **180**, 3205-3208 (1998).
32. M. Sobti *et al.*, Cryo-EM structures of the autoinhibited E. coli ATP synthase in three rotational states. *Elife* **5**, (2016).
33. W. Kuhlbrandt, Structure and function of mitochondrial membrane protein complexes. *BMC Biol* **13**, 89 (2015).
34. I. Liko *et al.*, Dimer interface of bovine cytochrome c oxidase is influenced by local posttranslational modifications and lipid binding. *Proc Natl Acad Sci U S A* **113**, 8230-8235 (2016).
35. E. Pebay-Peyroula *et al.*, Structure of mitochondrial ADP/ATP carrier in complex with carboxyatractyloside. *Nature* **426**, 39-44 (2003).
36. M. J. Berardi, W. M. Shih, S. C. Harrison, J. J. Chou, Mitochondrial uncoupling protein 2 structure determined by NMR molecular fragment searching. *Nature* **476**, 109-113 (2011).
37. E. R. Kunji, P. G. Crichton, Mitochondrial carriers function as monomers. *Biochim Biophys Acta* **1797**, 817-831 (2010).
38. M. Klingenberg, The ADP and ATP transport in mitochondria and its carrier. *Biochim Biophys Acta* **1778**, 1978-2021 (2008).

39. G. Hedger *et al.*, Lipid-Loving ANTs: Molecular Simulations of Cardiolipin Interactions and the Organization of the Adenine Nucleotide Translocase in Model Mitochondrial Membranes. *Biochemistry* **55**, 6238-6249 (2016).
40. L. M. Sparks *et al.*, ANT1-mediated fatty acid-induced uncoupling as a target for improving myocellular insulin sensitivity. *Diabetologia* **59**, 1030-1039 (2016).

**Acknowledgments:** The authors thank C. J. Schofield for access to a probe sonicator and the Robinson group for helpful discussions. **Funding:** DSC and CVR. are supported by the European Research Council grant no. 69551-ENABLE and a Wellcome Trust Investigator Award (104633/Z/14/Z). LAB was supported by a Human Frontier Science Program Long Term Fellowship and a Canadian Institutes for Health Research Postdoctoral Fellowship. KG was supported by a Wellcome Trust Senior Research Fellowship (090895/Z/09/Z) and a core award (090532/Z/09/Z). C.G. is supported by the JST (JPMJCR13M4), BINDS and MEXT (Kiban B: 17H03647). F.S. and S.K. are supported by the BBSRC (BB/M029573/1). A.G.S was supported by the NHMRC fellowship (1090408). **Author contributions:** D.S.C. produced the MPEEVs and preformed MS experiments. L.A.B and K.G. purified *E. coli* membranes and visualized vesicles by EM. D.W. established and executed the lipidomics. V.B.E. provided critical advice for proteomics. S.L.R., S.J.M, S.K and F.S performed MD simulations. TZBM provided critical support in establishing the MPEEV system. C.J. and C.G purified intact mitochondria and inner membrane samples. A.G.S provided critical review. D.S.C and C.V.R designed experiments, preformed data analysis and wrote the manuscript. **Competing interests:** Authors declare no competing interests. **Data and materials availability:** All data is available in the main text or the supplementary materials.

**Supplementary Materials:**

Materials and Methods

Figures S1-S16

Tables S1-S3

References (41-59)

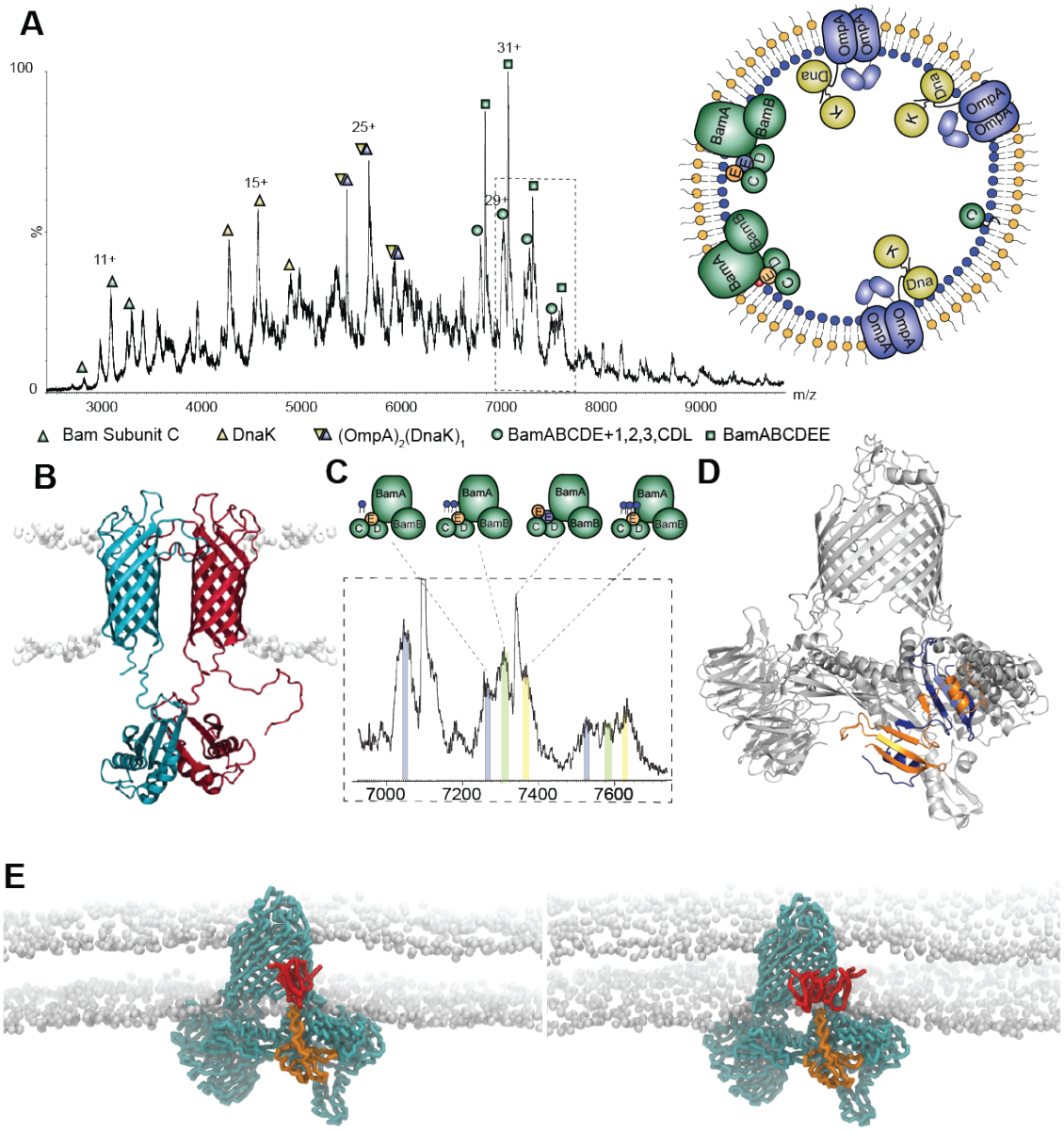


**Fig. 1. Protein complexes extruded directly from *E. coli* outer membranes** **A** Mass spectrum recorded at 400 V assigned to BamC, DnaK, DnaK:OmpA:pro-OmpA, and two states of the Bam complex with ***inset*** an outer membrane vesicle with complexes observed. **B** Model of the OmpA dimer (*15*) with the hydrophobic pro-sequence (red) a potential binding site for DnaK. **C** Expansion of the mass spectrum assigned to the Bam complex with monomeric BamE (Bam ABCDE) binding to one, two and three cardiolipins (grey, green, yellow respectively). **D** Atomic structure of BamE dimer (PDB: 2YH9) (orange and blue) docked into the Bam complex (PDB: 5D0O) with BamE monomer removed. **E** MD simulations of the BamABCDE complex (cyan) with monomeric BamE (orange) and two (lhs) and three (rhs) CDL molecules (red).

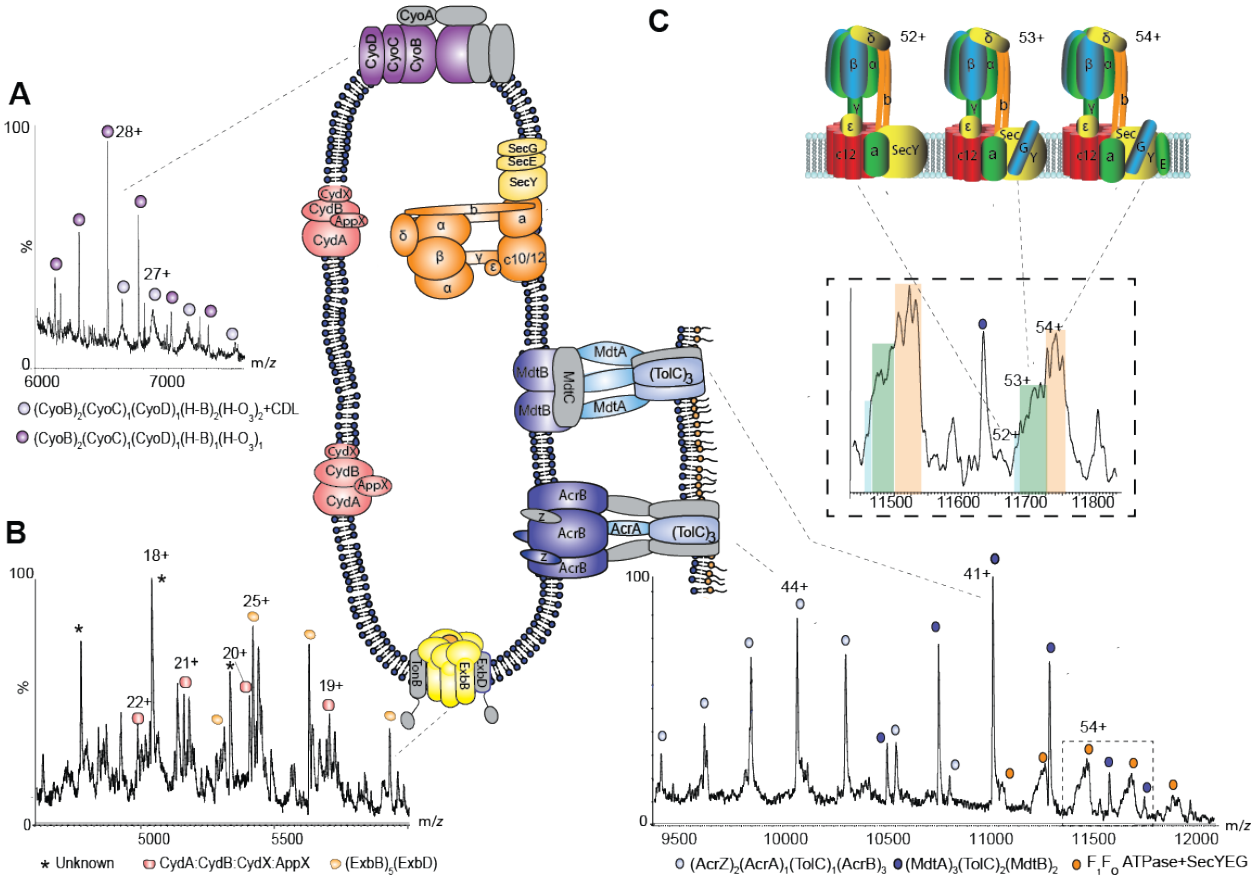


**Fig. 2. Regions of the mass spectrum recorded for inner membranes from *E. coli* yield cytochromes, the Ton complex multi-drug transporters and the intact ATP synthase in complex with the SecYEG translocon. A and B** Expanded regions of the spectrum assigned to the cytochromes *bo*$_3$ and cytochrome bd oxidase showing peak splitting due to binding of quinol and heme groups (fig. S8). The pentameric ExbB complex, with one copy of ExbD located in the center of the pore, forming part of the TonB complex is also observed (yellow). **C** High m/z region of the mass spectrum assigned to multidrug efflux pumps AcrAB and MdtAB and the intact ATP synthase. Expansion of the peaks assigned to the ATPase reveals binding of SecY (blue) SecYG (green) and SecYEG (orange) charge states 52+, 53+ and 54+ shown schematically.

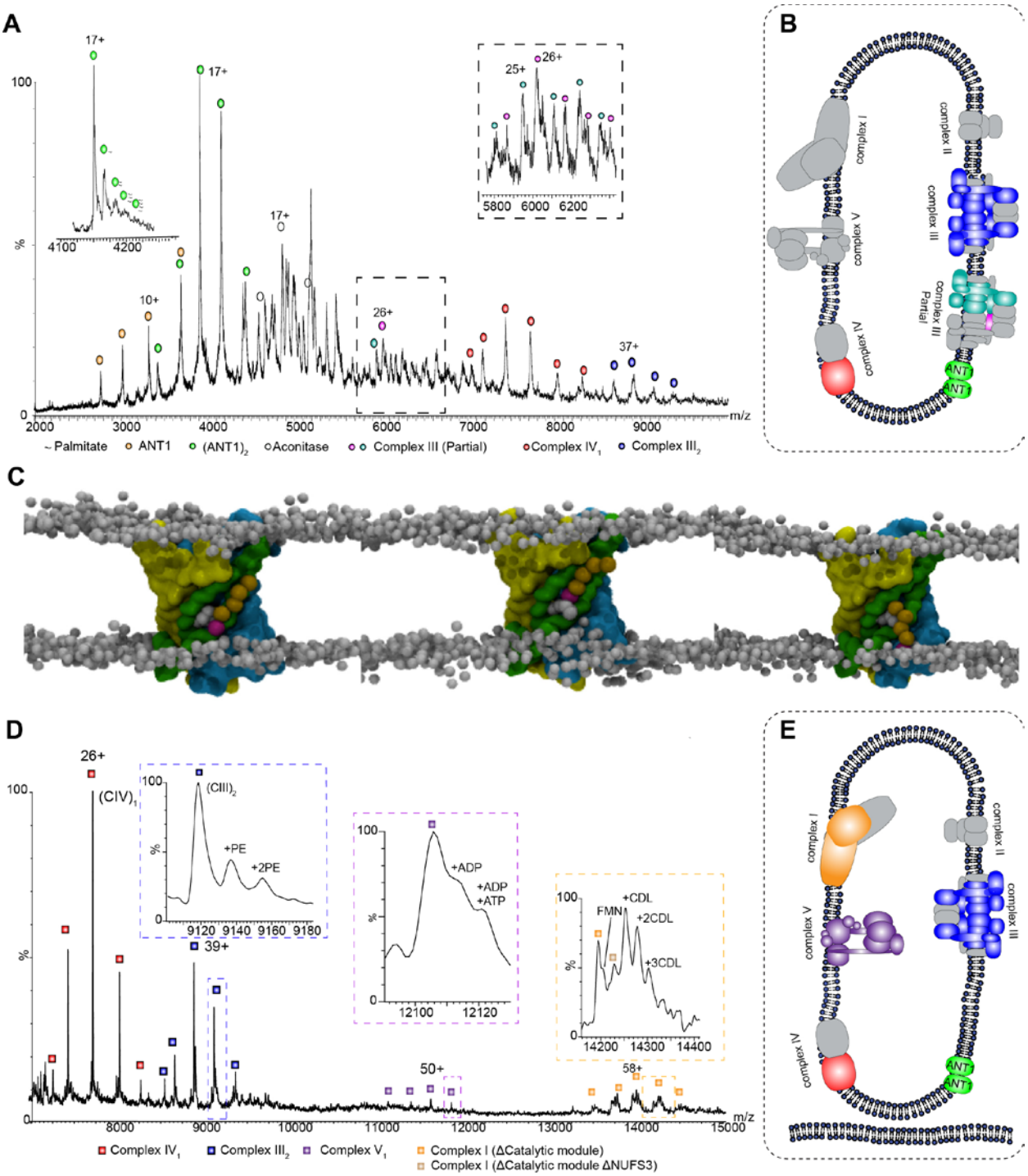


**Fig. 3. Intact Mitochondria and inner membranes yield complexes I, III, IV and V as well as the adenine nucleotide translocator 1 (Ant1) with palmitate transport through the dimer interface. A** Mass spectrum of inner membranes recorded at 400 V (expansion from 4,100 - 4,300 m/z inset), revealing multiple palmitate anions bound to the dimer of ANT1. Peaks in the MS recorded at 600 V (main panel) are assigned to Complexes III and IV as well as aconitase. **B** MD simulation of ANT1 after 2.1 μs, 2.5 μs and 2.6 μs (left to right) in an asymmetric membrane containing PC, PE, and CDL (only in the matrix leaflet). Protein surface is colored

according to the three pseudo repeats (R1; yellow, R2; green, R3; cyan) the charged palmitate headgroup (magenta) buries between helices 3 and 4. **C** Complexes I, III, IV and V are expelled form intact mitochondria. Intact complex V is observed with associated nucleotides, together with a dimer of complex IV and partial assemblies of complex 1 in the absence of the catalytic core but bound to FMN. Schematics represent membrane complexes assigned, color coded according to labels on the peaks.

# Supplementary Materials for

## Protein assemblies ejected directly from native membranes yield intact complexes for mass spectrometry

Dror S. Chorev[1], Lindsay A. Baker[2], Di Wu[1], Victoria Beilsten-Edmands[1], Sarah L. Rouse[3], Tzviya Zeev-Ben-Mordehai[2,#], Chimari Jiko[4], Firdaus Samsudin[5], Christoph Gerle[6,7], Syma Khalid[5], Alastair G. Stewart[8,9], Stephen J. Matthews[3], Kay Grünewald[2,10], and Carol V. Robinson[1,*].

Correspondence to: carol.robinson@chem.ox.ac.uk

**This PDF file includes:**

## Materials and Methods

### Outer and Inner Membrane Vesicle Preparation

Outer and inner membranes were prepared as described previously (*41*). Briefly, 0.5 L *E. coli* BL21 was grown in LB to OD 2.0 at 37 °C with 250 rpm shaking, before harvesting the cells by centrifugation at 4000xg for 10 min. Cells were resuspended in buffer A (50 mM Tris pH 7.4, 150 mM NaCl) and lysed with a constant flow cell disruptor at 8-12 kpsi. Cell debris was removed by centrifugation at 4000xg for 10 min, and membranes were harvested by ultracentrifugation in a Beckman SW32Ti rotor for 1 hr at 25000 rpm. The supernatant was removed and the membranes were resuspended in 5.8 mL of buffer A with 20% sucrose, before layering on a discrete sucrose gradient in buffer A (0.85 mL 55% sucrose, 11.4 mL 51% sucrose, 11.4 mL 45% sucrose, 7.8 mL 36% sucrose) and centrifuging for 17 h at 30000 rpm in a SW32Ti rotor. Outer and inner membranes were removed from the interface of the 55% and 51% and 45% and 36% sucrose layers respectively and washed twice in ~38 mL lysis buffer without sucrose by centrifuging at 25000 rpm for 1 hr in a SW32Ti. Membranes were then resuspended in 0.5-1 mL buffer A and stored at 4°C until further use.

### MPEEV Preparation

BHK-21 cells were grown in Glasgow MEM containing 10% FBS, 20 mM HEPES and 2% Triptose Phosphate Broth at 37 °C, 5% $CO_2$ 24 h before transfection, $15x10^6$ cells were seeded onto a T175 cell culture flask. Cells were transfected using 60 µg of selected DNA utilizing Lipofectamine 2000 according to the manufacturer's protocol. 2 h post transfections, cells were washed with PBS and media was changed with 2% FBS in GMEM. 24 h after transfection cells were washed and medium was replaced with serum free GMEM. 2 days following transfection, medium was collected and centrifuged at 30,000 rpm in a Beckman ultracentrifuge utilizing an SW32Ti rotor. The supernatant was then removed and vesicles were resolubilized in 500 mM Ammonium Acetate at pH 7.6.

### Preparation of mitochondrial membranes

Mitochondrial inner membranes were prepared as previously described (*42*). In brief, after careful removal of fat and connective tissues, bovine heart muscle of one fresh bovine heart was minced using a commercial meat mincer. A 600 g portion of minced meat was suspended on ice in 2,650 mL of 26 mM sodium phosphate buffer, pH 7.4, and homogenized for 10 min at 11,000

rpm in a Polytron PT3100D homogenizer, followed by centrifugation for 20 min at 2,800 rpm in a large-scale refrigerated centrifuge (Hitachi himac CR20G) using an R9A rotor at 4 °C. All supernatants were combined and centrifuged for 25 min at 4 °C and 8,000 rpm in a Hitachi Himac CR20G centrifuge using a R12AF rotor. The precipitate, suspended in 40 mM HEPES buffer (pH 7.8), 0.5mM EGTA/EDTA and 1mM DTT, was centrifuged for 30 min at 30,000 rpm in a P45AT rotor using a Hitachi Himac CP80WX ultracentrifuge. Finally, the precipitate was suspended in 40 mM HEPES buffer (pH 7.8), 2 mM $MgCl_2$, 0.5 mM EGTA/EDTA, 1 mM DTT, and the protein concentration adjusted to 26.8 mg/ml.

For outer and inner membrane preparations that were not separated, membranes were prepared in the same way but without the osmotic bursting and ultra-centrifugation steps.

**Sonication of Membranes for Native Mass Spectrometry**

Collected vesicles were diluted in 20 ml of 500 mM Ammonium acetate, and sonicated using a probe sonicator (Vibra-Cell VCX-500 Watt, Sonics) using maximal amplitude. Volume was then reduced to ~200 microliters using a 10-50 kDa cut-off concentrating tube (Milipore).

**Native Mass Spectrometry**

Native mass spectrometry experiments were carried out on a Q-Exactive Plus UHMR (*11*) modified to facilitate the transmission of high-energy species (*43*) and adapted for membrane proteins (*44*). The following parameters were used: Capillary Voltage - 1.6 kV, Dessolvation voltage- -200 V, Source fragmentation - 200 V, HCD energy - 0-300 V. HCD pressure was set to 6, the equivalent of $1.8x10^{-9}$ bar. EMR was set to on, C-trap entrance lens tune offset was set to 2, injection flatopole was set to 8 V, inter flatopole lens was at 6V, and bent flatopole at 4 V. Threshold was set to 3. Data was analysed using Xcalibur 2.2 (Thermo Fischer) and Masslynx 4.2 (Waters).

**Lipidomics**

MPEEVs in Ammonium Acetate were lyophilized by a vacuum concentrator (Savant SPD1010 SpeedVac Concentrator, Thermo Scientific). The lipid/protein mixture was then re-dissolved in 60% acetonitrile (ACN) by sonication for 10 min. For LC-MS/MS analysis, the lipids were separated on a C18 column (Acclaim PepMap 100, C18, 75 µm × 15 cm; Thermo Scientific) by Dionex UltiMate 3000 RSLC nano System connected to a hybrid LTQ Orbitrap mass spectrometer (Thermo Scientific) via a dynamic nanospray source. The buffers and gradient are

adapted from (*45*). Briefly, a binary buffer system was used with buffer A of ACN: $H_2O$ (60:40), 10 mM ammonium formate, 0.1% formic acid and buffer B of IPA: ACN (90:10), 10 mM ammonium formate, 0.1% formic acid. The phospholipids were separated at 40 °C with a gradient of 32% to 99% buffer B at a flow rate of 300 nl/min over 30 min. Typical MS conditions were a spray voltage of 1.8 kV and capillary temperature of 175 °C. The LTQ-Orbitrap XL was operated in negative ion mode and in data-dependent acquisition with one MS scan followed by five MS/MS scans. Survey full-scan spectra were acquired in the orbitrap (m/z 350 − 2,000) with a resolution of 60,000. Collision-induced dissociation (CID) fragmentation in the linear ion trap was performed for the five most intense ions at an automatic gain control target of 30,000 and a normalized collision energy of 38% at an activation of q = 0.25 and an activation time of 30 ms (*45, 46*).

**Protein identification and proteomics**

For identification of proteins, protein bands were excised from the gel and processed as described (*47*). Peptides were re-suspended in 0.1% Formic Acid and separated on an Ultimate 3000 UHPLC system (Thermo Fisher Scientific) and electrosprayed directly into a QExactive mass spectrometer (Thermo Fisher Scientific) through an EASY-Spray nano-electrospray ion source (Thermo Fisher Scientific). The peptides were trapped on a C18 PepMap100 pre-column (300 µm i.d. x 5 mm, 100 Å, Thermo Fisher Scientific) using solvent A (0.1% Formic Acid in water) at a pressure of 500 bar. The peptides were separated on an analytical column (75 µm i.d. packed in-house with ReproSil-Pur 120 C18-AQ, 1.9 µm, 120 Å, Dr Maisch GmbH) using a gradient (15% to 38% for 30 min, solvent B - 0.1% formic acid in acetonitrile, flow rate: 200 nL/min) for 15 min. The raw data was acquired in a data-dependent acquisition mode (DDA). Full scan mass spectra were acquired in the Orbitrap (scan range 350-1500 m/z, resolution 70000, AGC target 3e6, maximum injection time 50 ms). After the MS scans, the 10 most intense peaks were selected for HCD fragmentation at 30% of the normalized collision energy. HCD spectra were also acquired in the Orbitrap (resolution 17500, AGC target 5e4, maximum injection time 120 ms) with first fixed mass at 180 m/z. Charge exclusion was selected for 1+ and 2+ ions. The dynamic exclusion set to 5 secs. All peptides were manually validated. Peptide identification was done using the MASCOT Daemon client program.

**Electron cryo-microscopy**

Inner and outer membranes were applied to Quantifoil 2/1 holey carbon grids after glow-discharging for 1 min 30 s on high (30 W) in a PDC-002-CE Plasma Cleaner (Harrick Plasma Ithaca, United States), before blotting for 8 s by hand and plunging into a bath of propane/ethane with a manual plunger. Grids were stored under liquid nitrogen until imaging. EM data was recorded on either a TF30 or TF30 Polara (ThermoFisher/FEI), equipped with K2 direct electron detectors and Quantum energy filters (Gatan). Data was collected with SerialEM (*48*), with pixel sizes between 2 and 3 Å/pixel at the specimen level and the energy selecting slit set to 20 eV, as movies with 5 frames per second in counting mode at a dose rate of ~5$e^-$/unbinned pix/sec, giving an overall dose of ~ 10-20 $e^-/Å^2$ on the sample. Frames were aligned and averaged in SerialEM.

**Molecular Dynamics Simulations**

For the Bam complex, the model outer membrane was constructed using the CHARMM-GUI web server (*49*) based on the lipid composition of *E. coli* K12 (100% Re LPS in the upper leaflet; 90% POPE, 5% POPG and 5% cardiolipin in the lower leaflet (*49*). The structure of the $BamABCD(E)_2$ complex was generated by aligning the BamE dimer (PDB: 2YH9) (*50*) to the BamE subunit in the BamABCDE complex (PDB: 5D0O) (*16*) using PyMOL. The atomic structures of BamABCDE and $BamABCD(E)_2$ were converted to coarse-grained representations using MARTINI 2.2 force field with the ELNEDYN elastic network model utilised to maintain the secondary structure (*51*). These protein complexes were embedded into the membrane and overlapping lipids were removed. The standard MARTINI water molecules were added to solvate the system, while 170 mM $Ca^{2+}$ ions and 150 mM NaCl were used to neutralize the system. Energy minimisation was performed following the steepest descent protocol. A short 10 ns equilibration simulation was conducted with position restraints imposed on the protein. These restraints were then removed and three independent 5 μs simulations (starting with different initial velocity distributions) were run for each system. The temperature was maintained at 323 K using the velocity rescaling thermostat (*52*) and the pressure was kept at 1 atm using the Parrinello-Rahman barostat (*53*). All simulations were performed using the GROMACS 2018 software.

For ANT1, simulations were performed using the gromacs 4.6.7 (www.gromacs.org) package (*54*) with GPU acceleration. Initial atomistic coordinates for the ADP/ATP translocase (ANT1) PDB id 1OKC (*35*) were taken from the MemProtMD database and Martini v2.2 coarse grained

parameters were generated using the martinize.py script with an elastic network of 1 nm cutoff and a force constant of 500 kJ $mol^{-1}$ $nm^{-2}$. Two molecules of ANT1 were placed in the xy-plane 9 nm apart in a simulation box of 18 x 18 x 10 nm and POPC:POPE:CDL:PLM membranes were generated by self-assembly with the protein positionally restrained as described elsewhere. To achieve an asymmetric membrane CDL was added to one side only of the simulation box. Production runs were 5 μs each. Simulations were performed at 310 K using the V-rescale algorithm (*52*) and 1 tau using the Parrinello-Rahman barostat with semiisotropic coupling. Visualisation used Pymol (http://pymol.org) and VMD (*55*). Lipid density isosurfaces of phosphate particles in the reference frame of the protein were generated using the Volmap plugin of VMD.

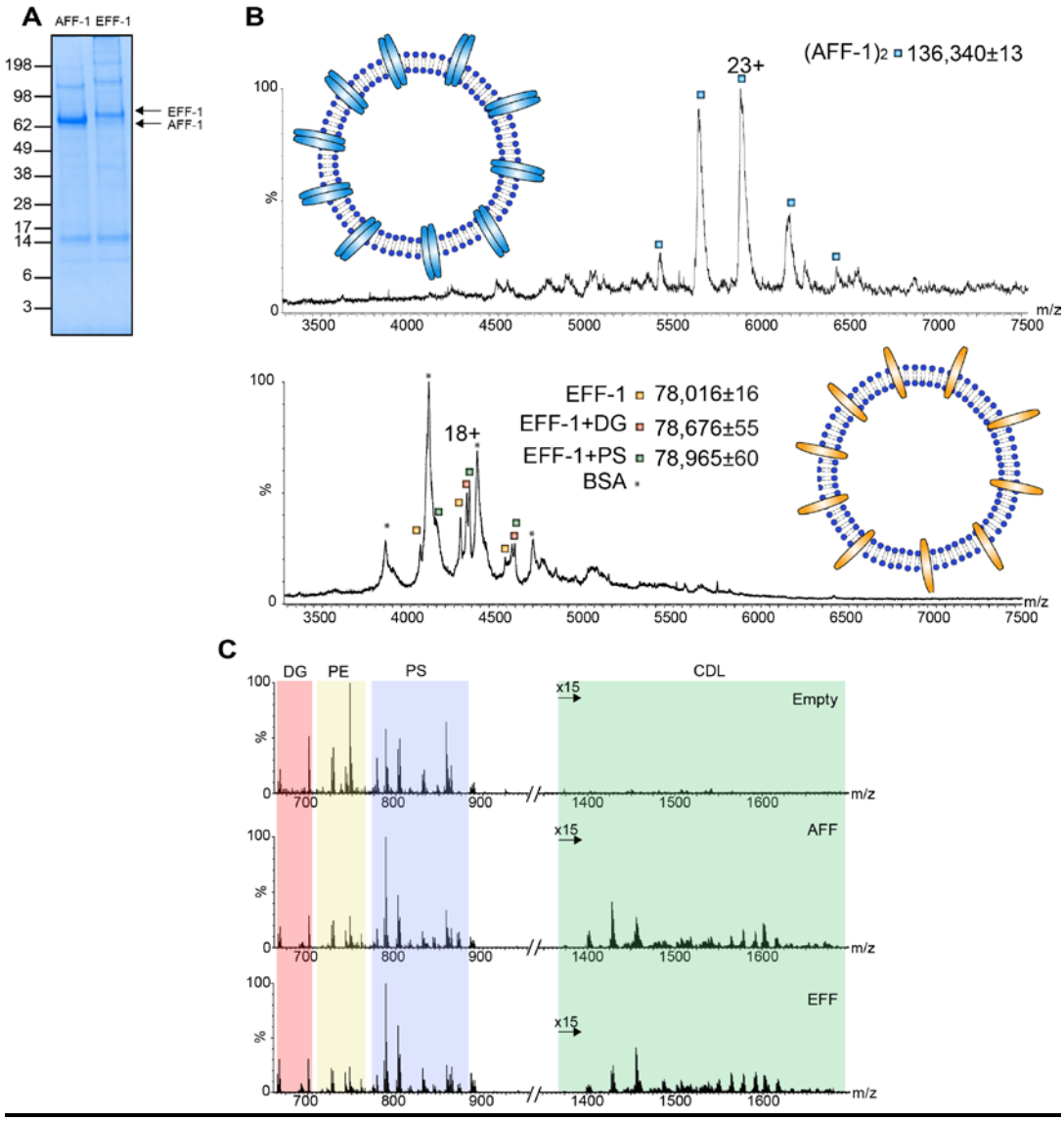


**Fig. S1. AFF-1 and EFF-1 ejected from membrane protein enriched extra cellular vesicles as a dimeric assembly and a lipid bound monomer. A** SDS-PAGE analysis of MPEEVs shows predominantly AFF-1 and EFF-1. **B** Predominant charge state series in the native mass spectrum of sonicated MPEEVs reveals dimeric AFF-1 and lipid bound monomeric EFF-1 with BSA carried over from cell growth serum. **C** Lipidomics comparison of empty and AFF-1 or EFF-1 containing vesicles reveals an increased concentration of cardiolipin upon overexpression of the two proteins. Different lipids are highlighted as follows: DG- Diacylglycerol (pink), PE- phosphatydilethanolamine (yellow), PS- phosphatydilserine (blue), CDL- cardiolipin (green).

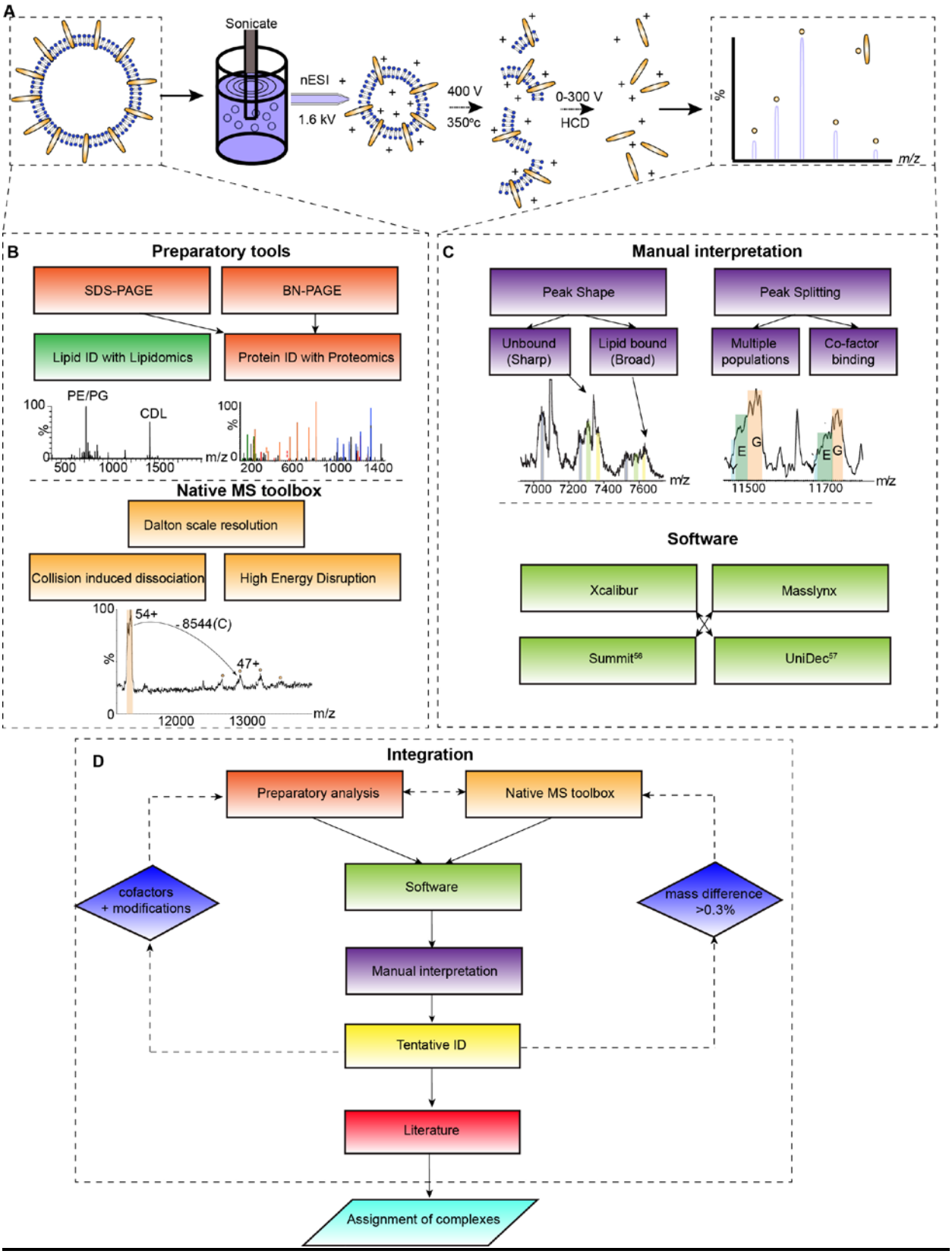
A
Sonicate
nESI
1.6 kV
400 V
350°c
0-300 V
HCD
%
m/z
B
Preparatory tools
SDS-PAGE
BN-PAGE
Lipid ID with Lipidomics
Protein ID with Proteomics
PE/PG
CDL
100
%
0
500
1000
1500
m/z
200
600
1000
1400
Native MS toolbox
Dalton scale resolution
Collision induced dissociation
High Energy Disruption
54+
8544(C)
47+
12000
13000
C
Manual interpretation
Peak Shape
Peak Splitting
Unbound (Sharp)
Lipid bound (Broad)
Multiple populations
Co-factor binding
7000
7200
7400
7600
11500
11700
E
G
Software
Xcalibur
Masslynx
Summit[56]
UniDec[57]
D
Integration
Preparatory analysis
Native MS toolbox
Software
cofactors + modifications
mass difference >0.3%
Manual interpretation
Tentative ID
Literature
Assignment of complexes

**Fig. S2. Procedure for preparation of sonicated lipid vesicles for MS (SOLVE-MS) and flowchart for assignment of complexes.** After vesicles are collected, they are subjected to sonication in 500 mM ammonium acetate within a 50 ml beaker using a probe sonicator and are concentrated in a 4 ml amicon (10-50 kDa molecular weight cut-off) to a volume of approximately 200 µl. Membrane vesicles are then introduced via nano-electrospray into a modified Q-Exactive mass spectrometer, optimised for high electric fields, and are ejected from their membrane environment to yield a mass spectrum of protein ensembles. Two different workstreams are employed to assign protein complexes. In the first standard preparatory tools are employed to identify lipids and proteins (including SDS PAGE gels, blue native gels and standard proteomics analysis of gel bands). For native MS, strategies to disrupt protein complexes are employed including CID and high-energy disruption. In the second stream, peaks in the mass spectrum are first subjected to manual inspection to define peak shape (heterogeneous lipid binding) or peak splitting (cofactor binding). Software tools (*56, 57*) are then employed to further assign peak series and to obtain mass measurements. These work streams are then integrated and a tentative assignment is reached. Extensive literature searching is then employed to query masses against anticipated complexes reported previously. In some cases assignments are rejected as they do not satisfy the stringent mass error limit imposed ± ~ 0.3 %. Differences in established subunit stoichiometry (e.g. ANT1), cofactor binding (cytochrome bd1) or interactions between complexes (SecYEG ATPase) are then considered.

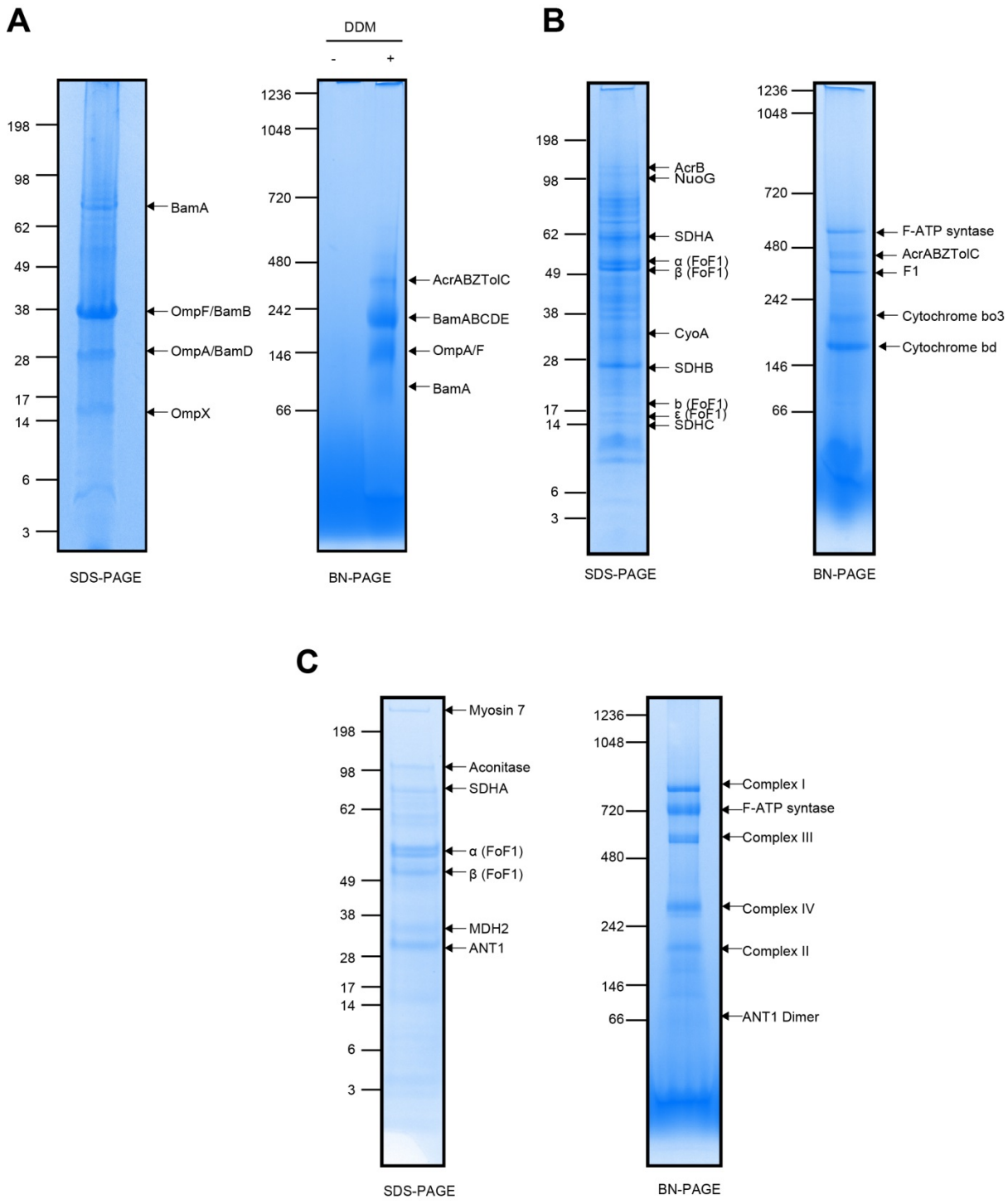


**Fig. S3. Native and denaturing PAGE analysis of whole membrane fractions.** SDS and BN-PAGE analysis of (**A**) *E. coli* outer membranes (**B**) *E. coli* inner membranes and (**C**) Bovine heart mitochondrial inner membranes. For SDS-PAGE analysis, proteins were boiled in sample buffer and run on a 4-12% NuPage bis-tris gel. For native gel analysis, proteins were incubated

for 20 mins with 0.5% DDM on ice before being supplemented with native sample buffer and separated on 4-12% Native Page bis-tris gels. Gel kits and running buffers were form Life Technologies.

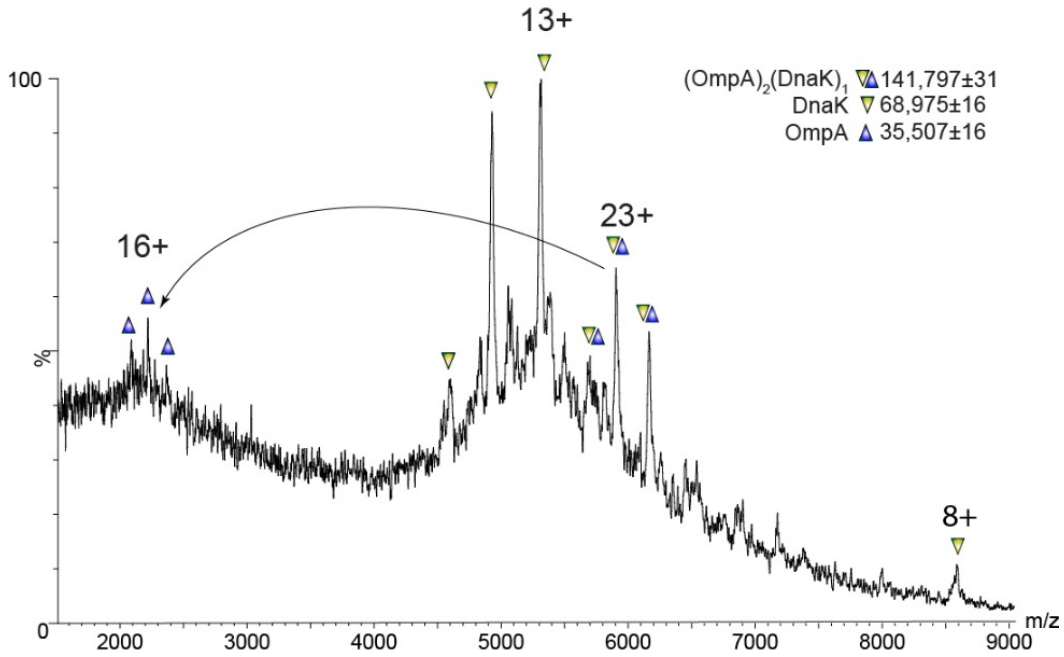


**Fig. S4. High-energy disruption of a 143 kDa complex releases full-length OmpA and DnaK.** Mass spectrum acquired on a Waters Synapt HDMS G1 instrument, with cone, trap and transfer voltages set to 200 V (Total of 600 V). Dissociation of full-length OmpA is achieved by generating an unfolded highly-charged monomer.

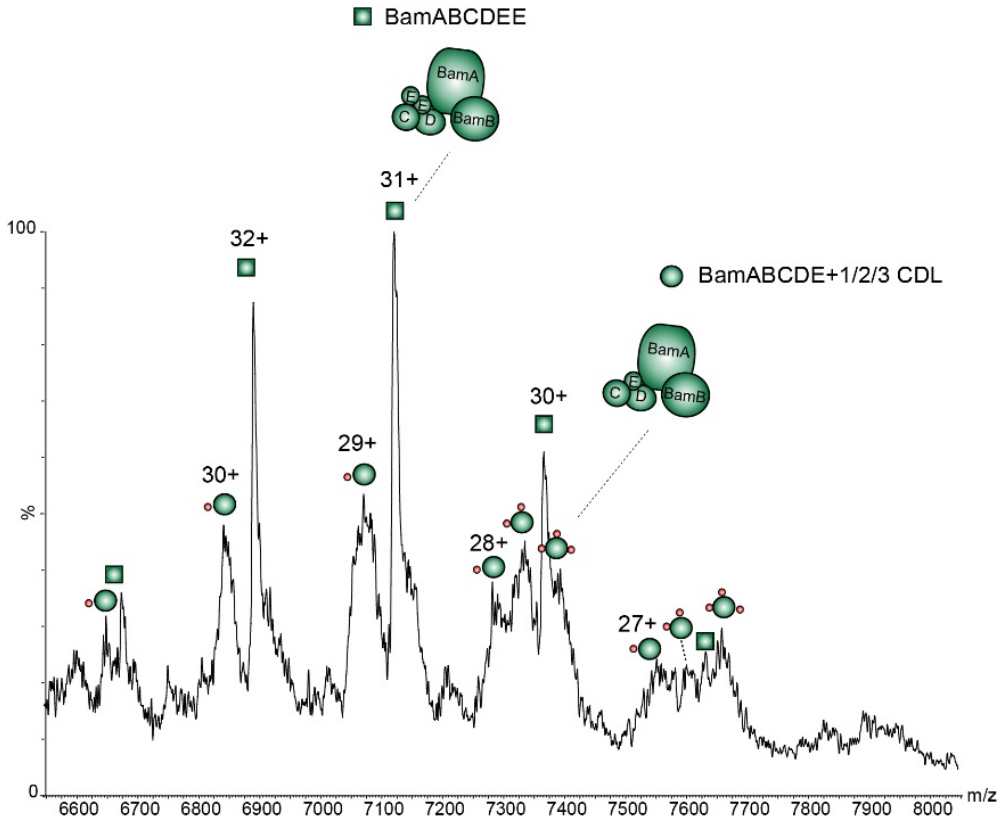


**Fig. S5. BamABCDE can bind up to three cardiolipins.** Expansion of the 6400-8100 m/z region of the spectrum shows a charge state series corresponding to the intact pentameric Bam complex with associated cardiolipins. Low charge states (28+) reveal additional peaks corresponding to binding of up to three cardiolipins. CDL average mass was 1492.9 Da indicative of CDL 76:14.

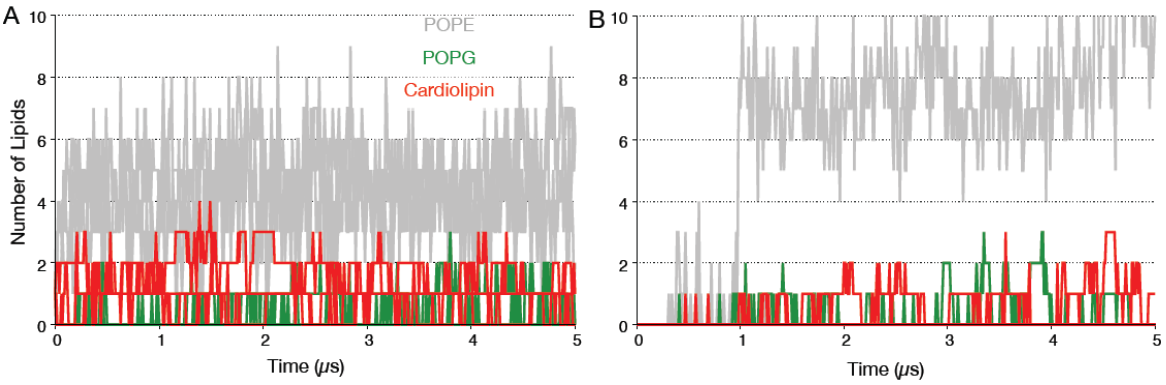


**Fig. S6. Molecular dynamics simulations suggest that BamE within the Bam complex is capable of binding up to three CDL.** The Bam complex was simulated at 323 K for 5 µs. CDL was randomly distributed within the membrane to avoid bias. POPE is labelled in grey, POPG in green and CDL in red. A contact is defined as being within 6 Å. **A** A single subunit of BamE within the complex is capable of binding a maximum of three CDL throughout the simulation and is preferred over POPG. **B** BamE dimers within the complex do not make stable lipid binding interactions.

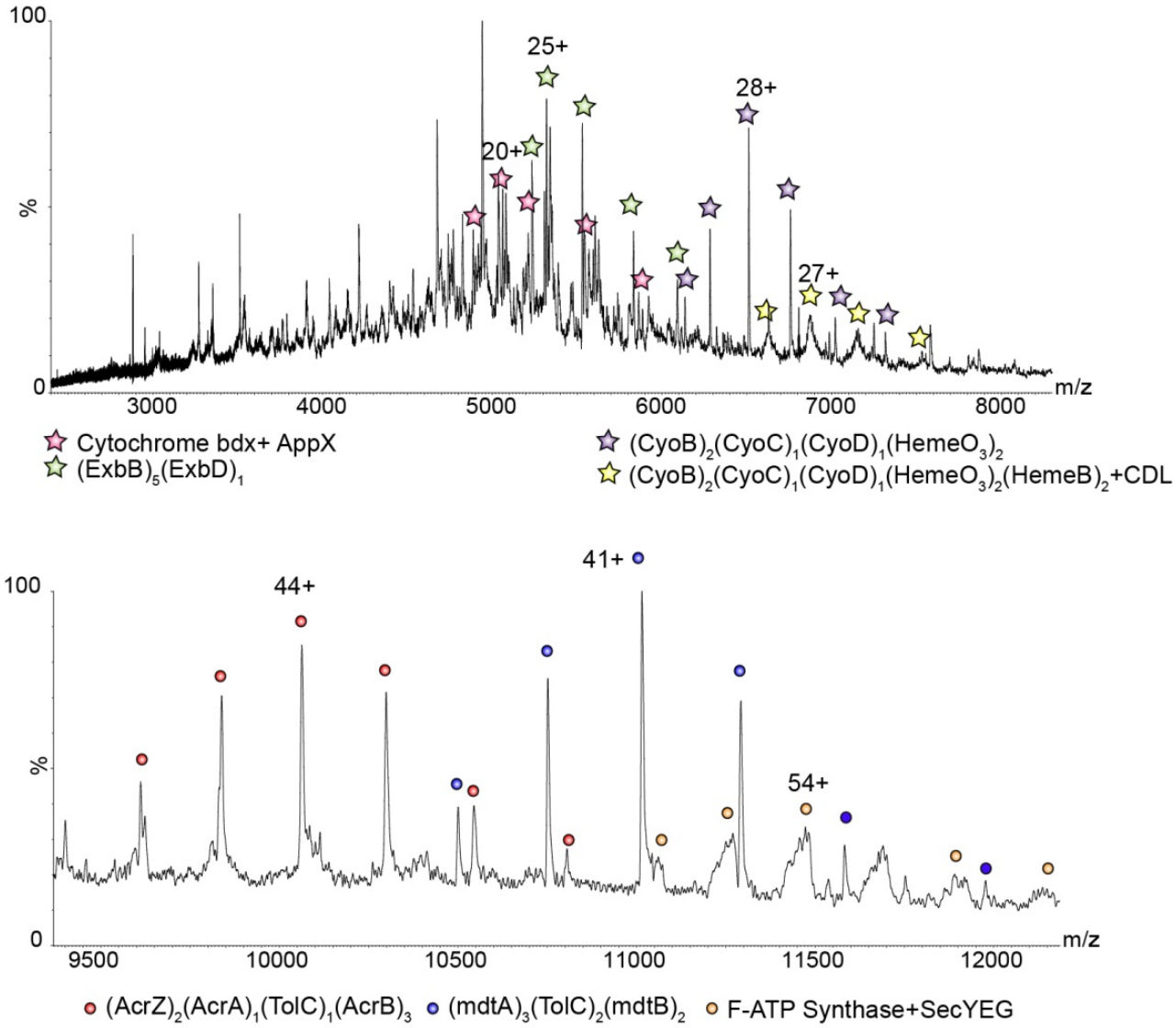


**Fig. S7. Full spectra recorded for *E. coli* inner membrane proteins.** Two cytochromes *bo*$_3$ and Cybdx, as well as the TonB complex (ExbB/D), are preserved in part (upper spectrum) and subcomplexes of two efflux pumps and the ATP synthase bound to SecYEG are observed (lower spectrum).

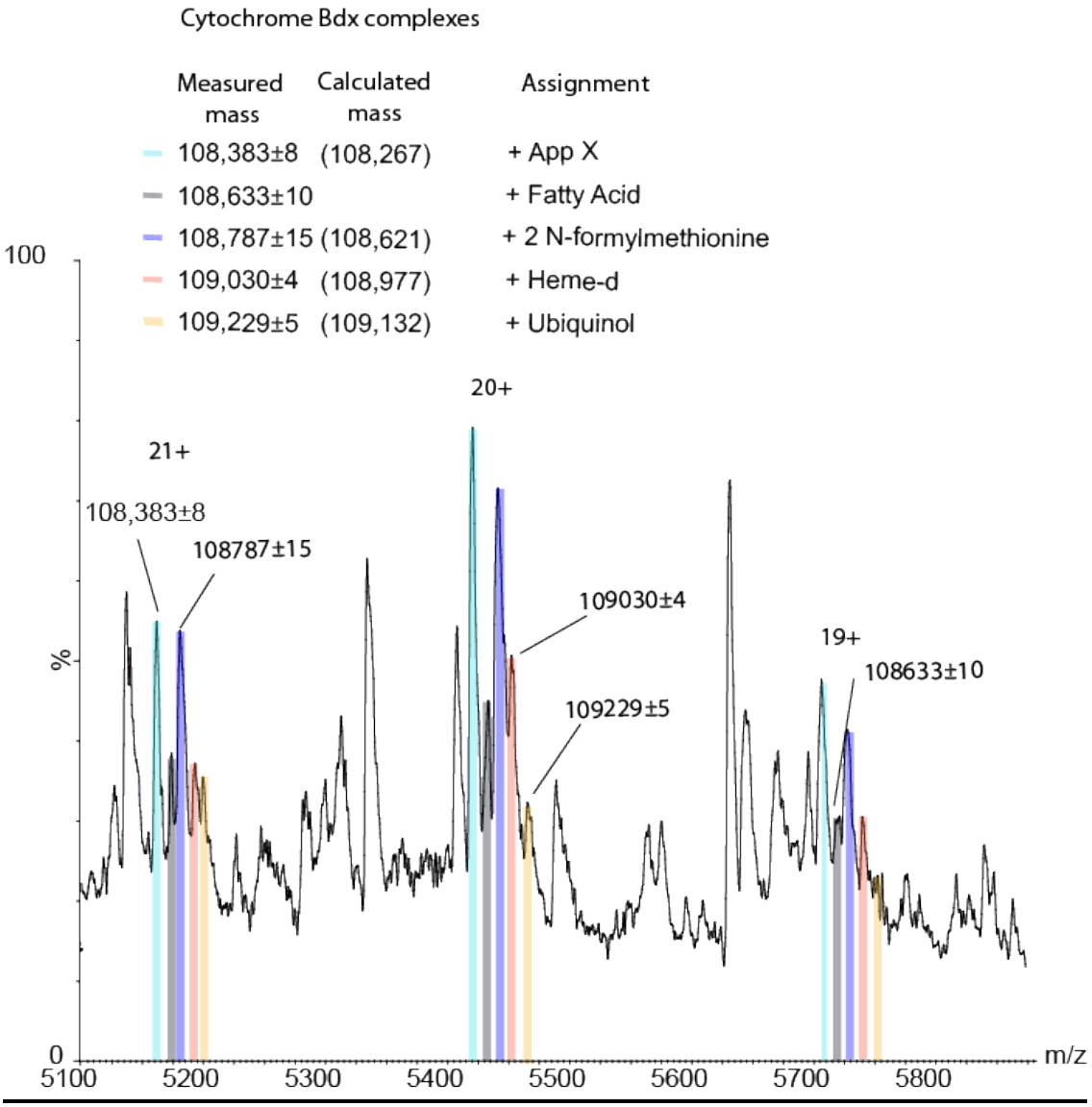


**Fig. S8. Native MS reveals co-factor and AppX binding to Cytochrome bdx.** Expansion of the 5,100-5,900 m/z range shows extensive peak splitting whereby the complex Cytochrome bdx is associated with AppX (aqua) and bound to an unknown small molecule (grey ~250 Da) likely to be a fatty acid. The complex is also modified with 2 N-formylmethionines (blue) and bound either to heme-d (pink) or ubiquinol (orange). Calculated masses are in brackets and peaks are color-coded according to their assignment.

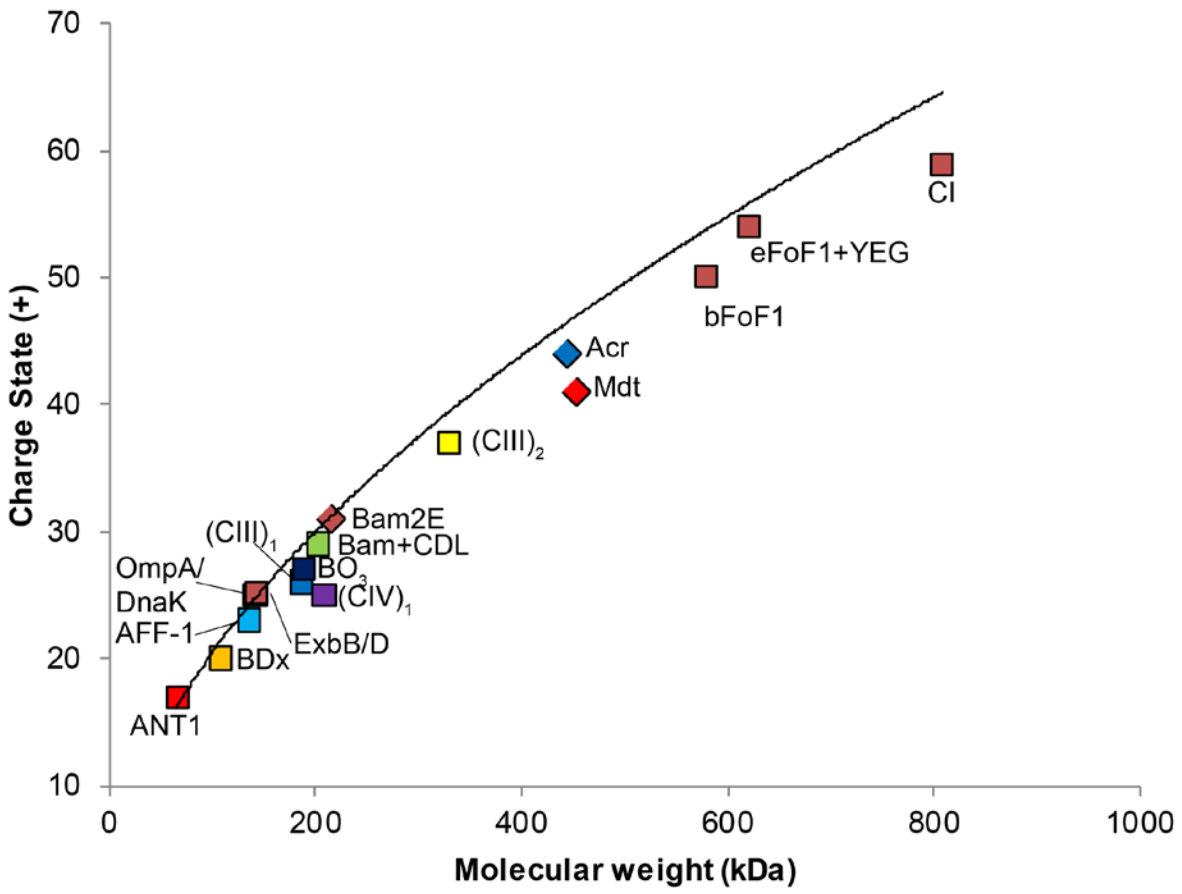


**Fig. S9. Average charge state plotted against the molecular mass of the membrane protein complex is indicative of established membrane protein charge reduction.** The different complexes assigned here, summarized in Table 4, were plotted with their molecular mass against their observed average charge state. Expected charge states were calculated using the following equation- $z=1.638xM^{0.5497}$ (black line). The average charge states of most membrane protein complexes are beneath the line, as observed previously for membrane proteins released from detergent micelles (*58*). The position of Mdt implies that it has undergone further gas phase dissociation than Acr for example.

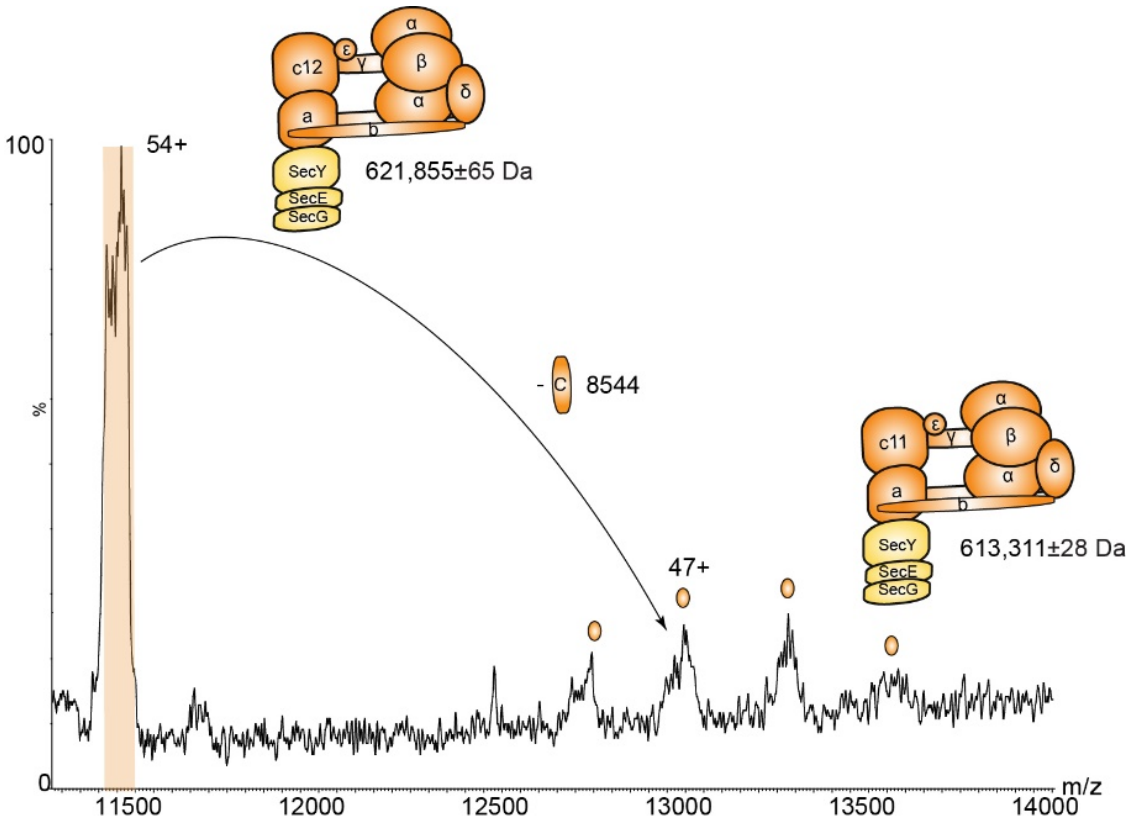


**Fig. S10. Collision induced dissociation of *E. coli* $F_OF_1$ ATP synthase ejects the membrane embedded subunit c.** m/z 11,515 was isolated using the quadrupole with a 100 Da window and the HCD collision energy was increased to 300 V giving a total of 700 V. The stripped complex is consistent with dissociation of a c-subunit and is in contrast to spectra recorded for rotary ATPases released from detergent micelles, in which peripheral subunits are lost preferentially (*59*) .

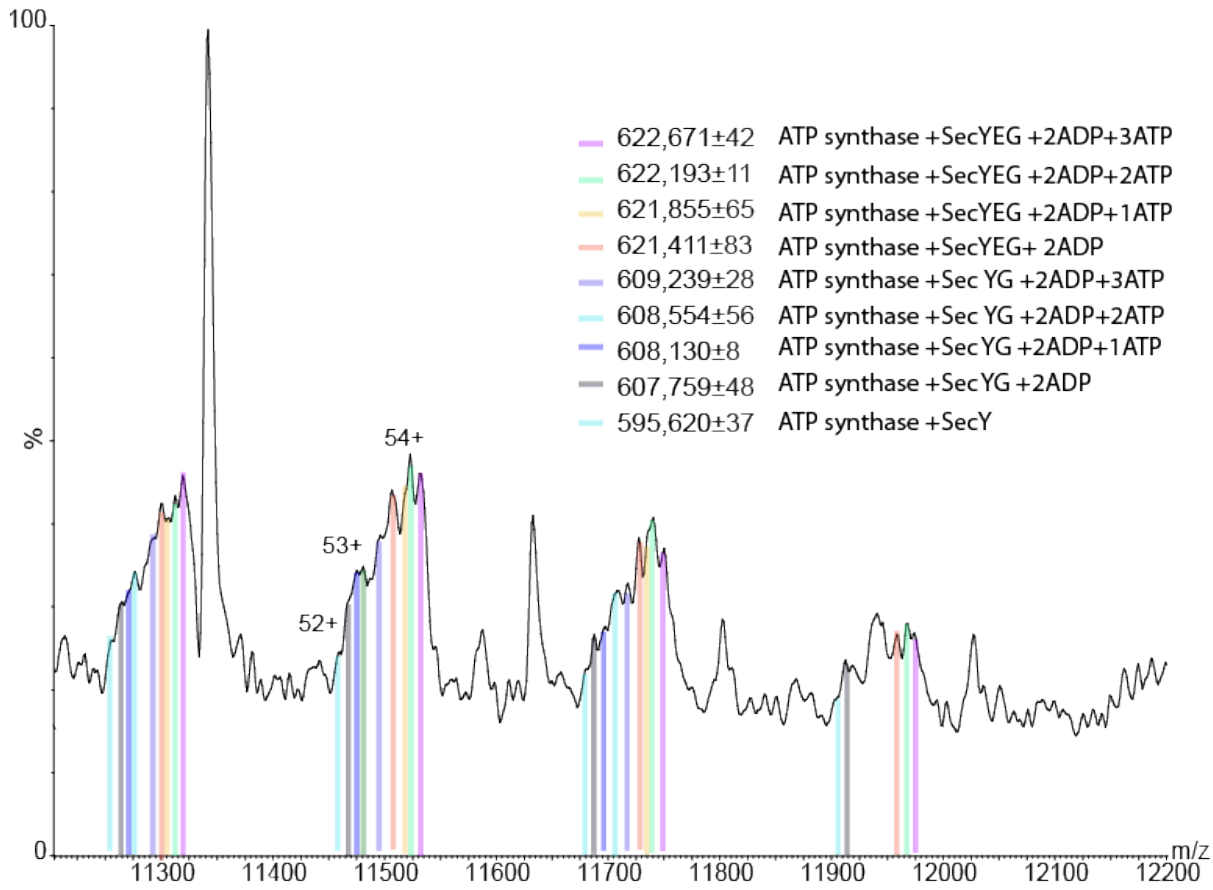


**Fig. S11. High-resolution mass spectrometry of the *E. coli* FoF$_1$ ATP synthase reveals molecular details of interactions.** Expansion of 11,200-12,200 m/z region shows extensive peak splitting. Three major populations are observed and assigned to SecY-bound ATP synthase with a additional populatiosn bound to SecG and SecE with 1-3 additional nucleotides, and a third population containing all SecYEG components bound to the ATP synthase, with a total of 5 bound nucleotide at the highest observable mass. In brackets is the expected mass.

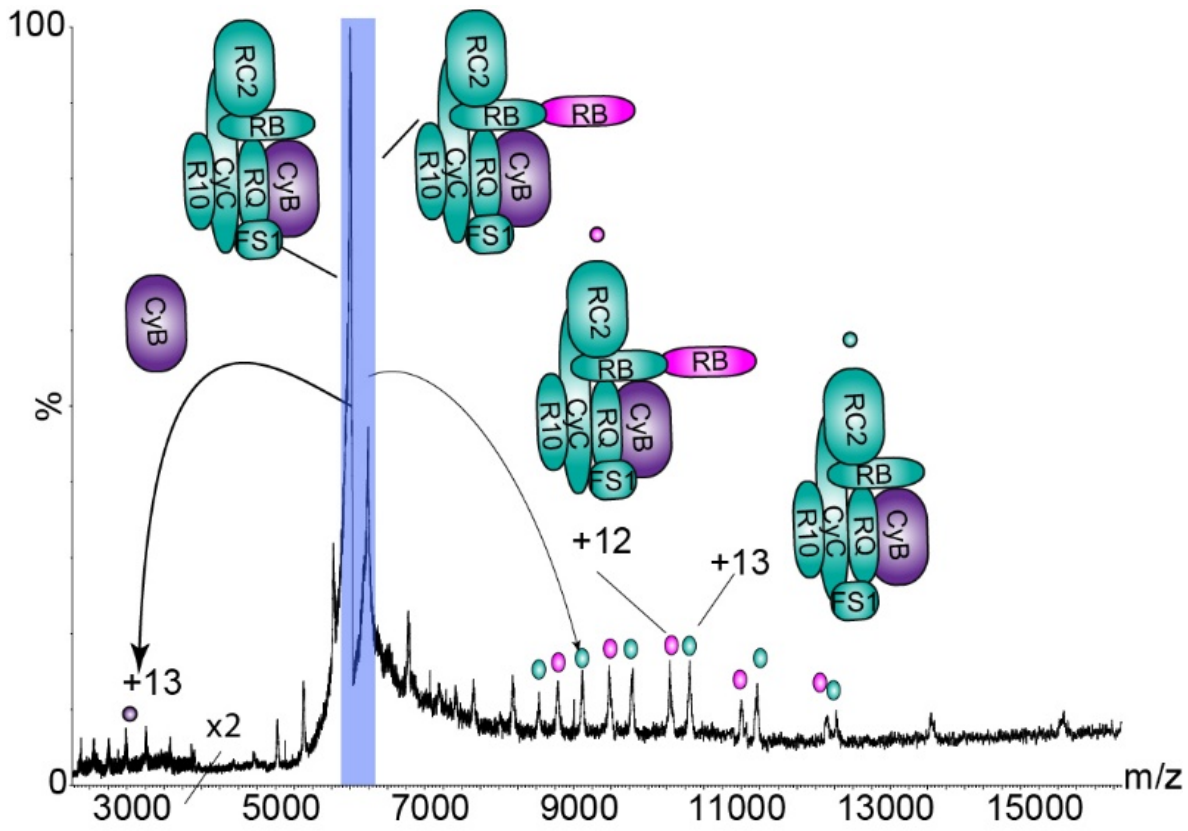


**Fig. S12. CID of two complexes that overlap in the mass spectra mitochondrial inner membranes from *Bos taurus* confirms that they are derived from Complex III.** An unfolded dissociation product Cytochrome B (42.5 kDa) is detected at low m/z (intensity multiplied by a factor of 2) and stripped complexes differing by 13 kDa, observed at high m/z, correspond to the mass of UQUCRB confirming that both these products are derived from Complex III assemblies.

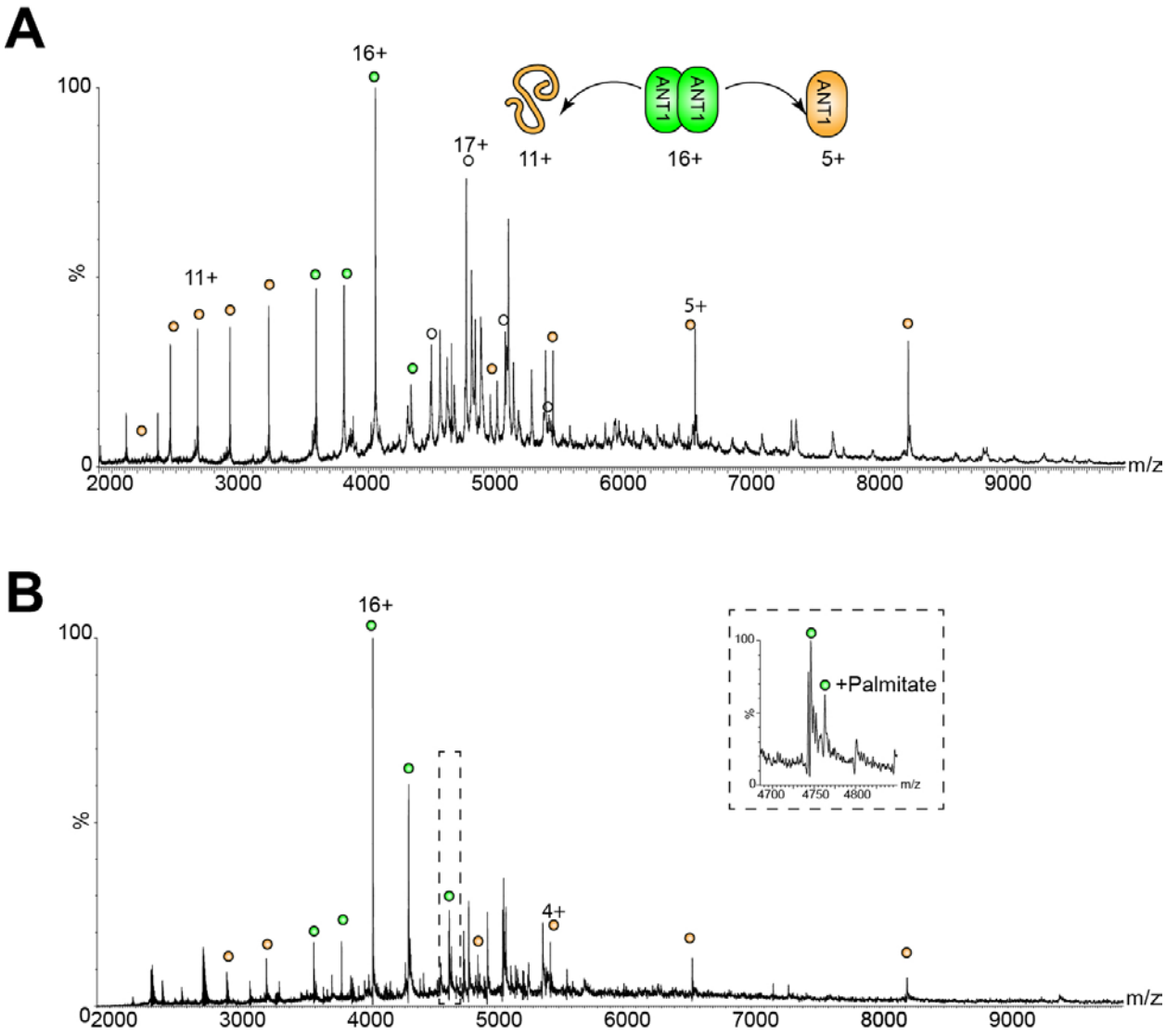


**Fig. S13. ANT1 is predominantly dimeric when ejected directly from bovine mitochondrial membranes.** Mass spectra recorded at 600 V from sonicated, inverted, separated inner membranes (A) and sonicated unseparated non-inverted bovine inner and outer membranes (B) show ANT1 is dimeric in both membranes and that Palmitate is bound to charge states assigned to the dimer in both cases. Inset expansion of the 14+ charge-state of unseparated non-inverted membranes.

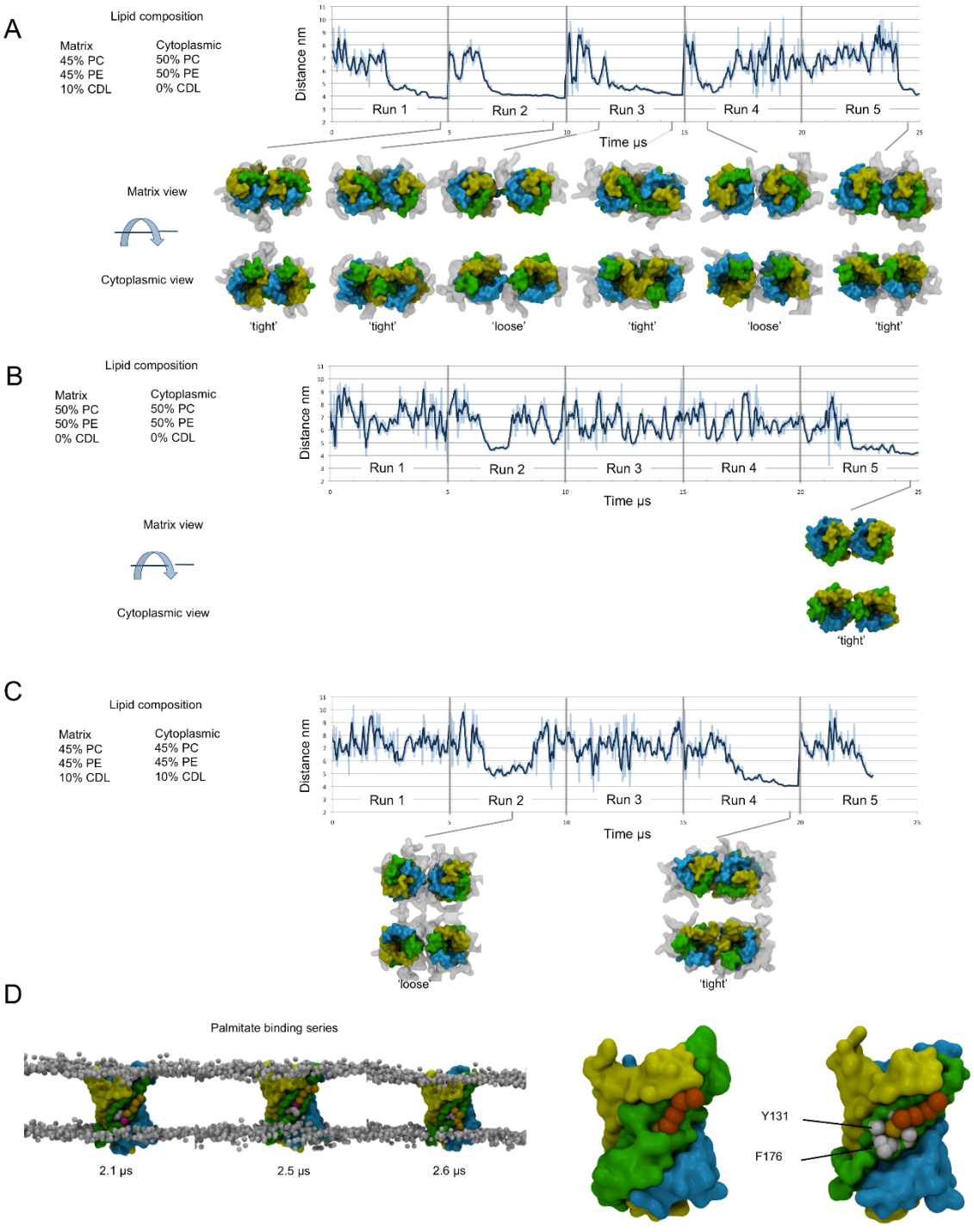


**Fig. S14. Molecular dynamics simulations of ANT1 in model mitochondrial inner membranes. A-C** Modulation of ANT1 dimer formation by the leaflet distribution of CDL. Three membrane compositions were tested in which CDL was present in the matrix leaflet **A**, no

leaflets **B** and both leaflets **C** of the membrane as indicated. The distance between each monomer over time for 5 independent 5 μs trajectories is shown. The 5 trajectories were concatenated for analysis. Snapshots of dimers formed corresponding to the timepoints as indicated are shown from both the cytoplasmic and matrix views. The protein is shown as a surface and coloured according to the pseudo repeats (repeat 1 yellow, repeat 2 is green and repeat 3 cyan). CDL within 1 nm of the protein is shown as a transparent grey surface. A dimer is considered 'tight' when both the matrix and cytoplasmic sides of ANT1 are in close contact. **D** Binding of palmitate to ANT1. The longest residence time observed for palmitate during a single simulation (coloured orange) was 0.4 μs in which the charged headgroup (coloured magenta) buries between helices 3 and 4, sitting above residues Y131 and F176 (grey spheres). The positions of lipid headgroup particles are shown as grey spheres.

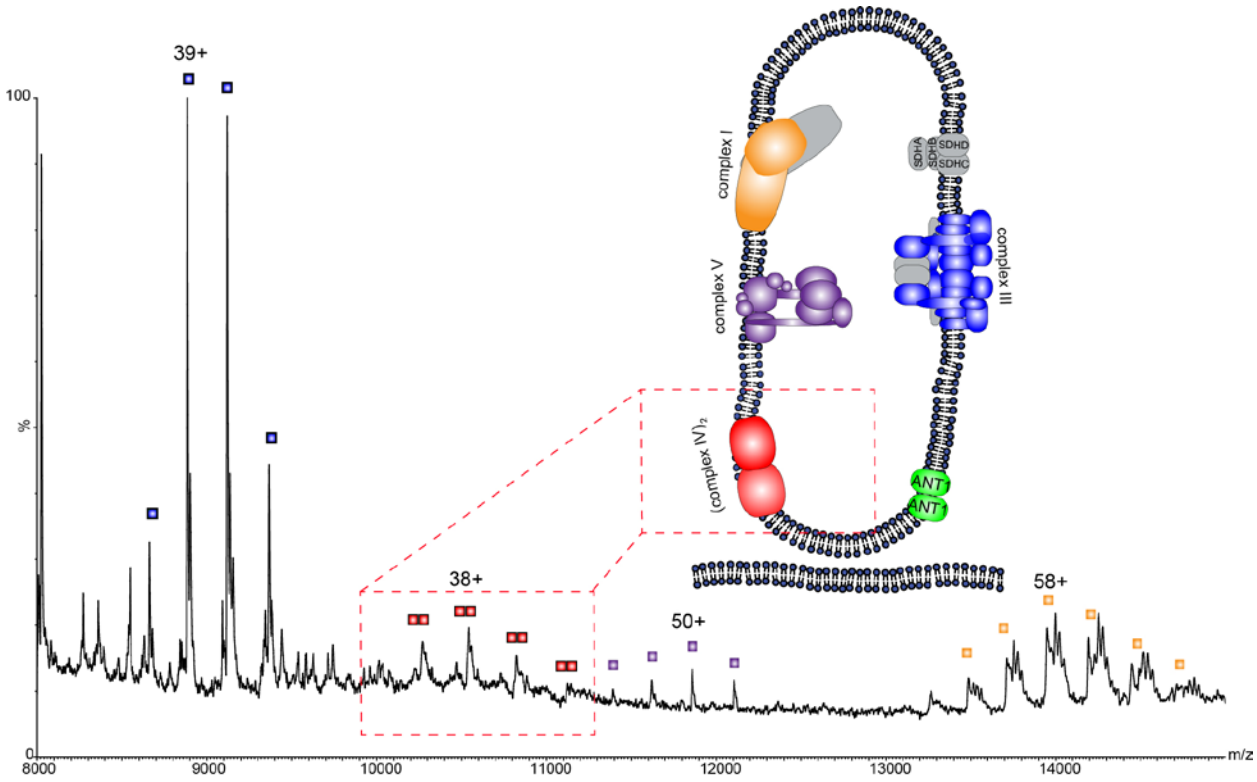


**Fig. S15. Quadrupole isolation of the 8,000-15,000 m/z range confirms the existence of a CIV dimer.** To enhance the details in the higher m/z region of the spectrum, the quadrupole window was reduced from 1,000-20,000 m/z to 8000-15,000 thereby allowing observation of a protein complex with a mass twice that of a CIV monomer assigned as a CIV dimer with associated lipids.

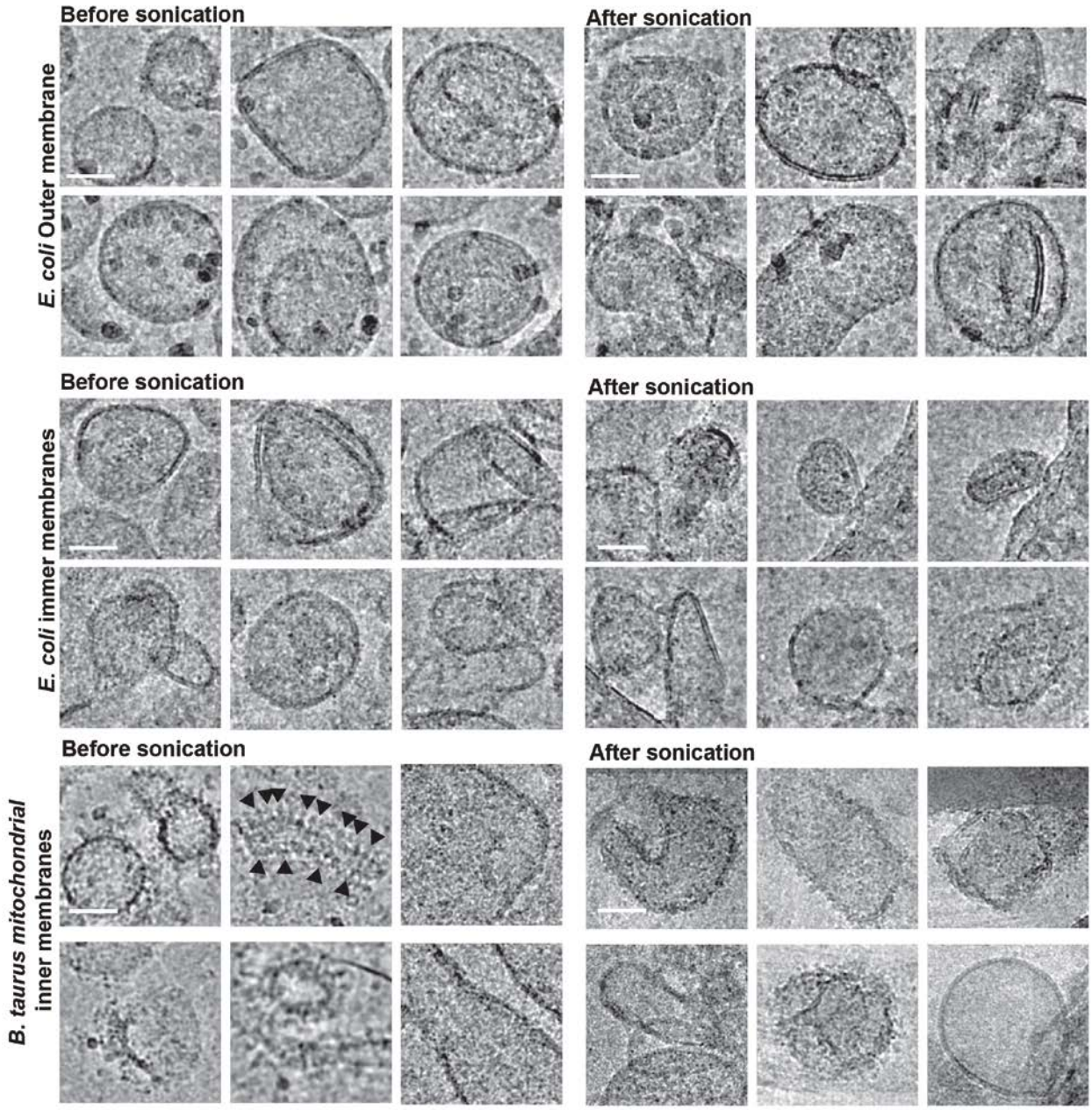


**Fig. S16. Electron Cryo-microscopy of vesicles before and after sonication.** Inner and outer *E. coli* membranes and *B. taurus* mitochondrial membranes were sonicated and visualized by EM. For inner and outer *E. coli* membranes proteins can be seen on the inside and outside of the vesicles. *B. taurus* are inverted as the F1 heads of the ATP synthase (marked with black arrows) can be seen pointing outwards. Scale bar is 50 nm.

**Table S1. Masses and identities of proteins and protein complexes from the outer membrane of *E. coli*.**

| Subunit/Complex<br>OmpA:proOmpA+DnaK | Expected mass (Da) | Measured mass (Da) | Mass difference (Da) | Mass difference (%) |
|---|---|---|---|---|
| DnaK | 69,115 | 69,148±55 | 33 | 0.047 |
| OmpA | 35,172 | | | |
| Pro OmpA | 37,201 | | | |
| DnaK:proOmpA:OmpA (+ADP) | 141,948 | 141,797±31 | -151 | 0.10 |
| Subunit/Complex<br>Bam complex | Expected mass (Da) | Measured mass (Da) | Mass difference | |
| BamA | 88,426* | | | |
| BamB | 40,643*<br>40,663* | | | |
| BamC | 35,163*<br>35,183* | | | |
| BamD | 26,583*<br>26,603 * | | | |
| BamE | 12,383*<br>11,268 (-tag)<br>12,413*<br>11,298 (-tag) | | | |
| BamABCDE+CDL | 203,218*-Light<br>202,103 (-tag)<br>203,288*-Heavy<br>202,179 (-tag) | 203,848±19 (1492 cdl) | 177 | 0.087 |
| BamABCDEE | 213,471 | 213,549±29 | 78 | 0.036 |

*Expected mass based on measurements reported previously (*17*). Heavy and light represent the masses of subunits bound to fatty acids with different chain lengths.

**Table S2. Masses and identities of inner membrane proteins and protein complexes from *E. coli.***

| Subunit/Complex<br>Mdt efflux pump | Expected mass | Measured mass | Mass difference (Da) | Mass difference (%) |
|---|---|---|---|---|
| MdtA | 42,178 | | | |
| MdtB | 112,078 | | | |
| MdtC | 111,010 | | | |
| TolC | 51,454 | | | |
| 3xMdtA 2xMdtB 2xTolC | 453,598 | 453,646±7 | 48 | 0.01 |
| Subunit/Complex<br>Acr efflux pump | Expected mass | Measured mass | Mass difference (Da) | Mass difference (%) |
| AcrA | 113,574 | | | |
| AcrB | 42,197 | | | |
| TolC (outer membrane) | 51,454 | | | |
| AcrZ | 5,300 | | | |
| 2xAcrZ 1xAcrA 1xTolC 3xAcrB | 444,973 | 444,922±6 | 51 | 0.011 |
| Subunit/Complex<br>TonB complex | Expected mass | Measured mass | Mass difference | |
| ExbA (TonB) | 26,094 | | | |
| ExbB | 26,287 | | | |
| ExbD | 15,227 | | | |
| 5xExbB 1xExbD | 146,662 | 146,333±28 | 329 | 0.2 |
| Subunit/Complex<br>ATP-synthase/SecYEG | Expected mass | Measured mass | Mass difference | |
| α | 55,222 | | | |
| β | 50,325 | | | |
| γ | 31,577 | | | |
| δ | 19,332 | | | |
| ε | 15,068 | | | |
| a | 30,303 | | | |
| b | 17,264 | | | |
| c | 8,256<br>N-Formylated- 8,284 | | | |

| | | | | |
|---|---|---|---|---|
| SecY | 48,512 | | | |
| SecE | 13,643 | 13,652 | 9 | 0.065 |
| SecG | 11,365 | | | |
| ATP synthase holo-complex | 546,857 (12c-formyl) | 595-622kDa | | |
| Holocomplex+SecY | 595,369 | 595,620±37 | 251 | 0.042 |
| Holocomplex+SecY+SecG +(2 ADP) | 607,588 | 607,759±48 | 171 | 0.028 |
| Holocomplex+SecYEG | 621,231 | 621,411±83 | 180 | 0.029 |
| Subunit/Complex<br>Cytochrome bd | Expected mass | Measured mass | Mass difference (Da) | Mass difference (%) |
| CydA | 58,205 | | | |
| CydB | 42,423 | | | |
| CydX | 4,042 | | | |
| AppX | 3,597 | | | |
| Heme B558 | 617 | | | |
| Heme B595 | 617 | | | |
| Heme d | 710 | | | |
| Ubiquinol | 865 | | | |
| Cytochrome bdx(+AppX) complex | 108,267 | 108383 ± 8 | 116 | 0.1 |
| Bdx+AptX+2N-formylmethionine | 108,621 | 108,633 ± 10 | 12 | 0.011 |
| Bdx+AptX+Heme d | 108,977 | 109,030 ± 4 | 53 | 0.048 |
| Bdx+AptX+Ubiquinol | 109,132 | 109,229 ± 5 | 97 | 0.088 |
| Subunit/Complex<br>Cytochrome *bo*$_3$ | Expected mass | Measured mass | Mass difference (Da) | Mass difference (%) |
| CyoA | 32,218 | | | |
| CyoB | 74,368 | | | |
| CyoC | 22,623 | | | |
| CyoD | 12,029 | | | |
| HemeO | 838.8 | | | |
| Heme B | 616.487 | | | |
| 2xCyoB 1xCyoC 1xCyoD 2xHemeO3 | 185,064 | 185,096±5 | 32 | 0.017 |
| 2xCyoB 1xCyoC 1xCyoD 2xHemeB 2xHemeO 1xCDL | 187,528 (1.4-1.6 CDL) | 188,103±4 | 575 | 0.311 |

**Table S3. Masses and identities of inner mitochondrial membrane proteins and protein complexes from *Bos taurus.***

| Subunit/Complex<br>ANT1 Dimer | Expected mass (Da) | Measured mass (Da) | Mass difference (Da) | Mass difference (%) |
|---|---|---|---|---|
| ANT1 (+3 Succinilation reported in mouse – uniprot database) | 33,187 | 33,195±11 | 8 | 0 |
| 2xANT1 | 66,374 | 66,387±13 | 15 | 0 |
| Subunit/Complex<br>Aconitase | Expected mass | Measured mass | Mass difference (Da) | Mass difference (%) |
| Aconitase | 82,401 | 82,635±9 | 234 | 0.2 |
| Subunit/Complex<br>Complex III | Expected mass | Measured mass | Mass difference (Da) | Mass difference (%) |
| UQCRC1 | 49,212 | | | |
| UQCRC2 | 46,523 | | | |
| UQCRH | 9,175 | | | |
| UQCRB | 13,345 | | | |
| UQCR10 | 7,326 | | | |
| UQCR11 | 6,520 | | | |
| UQCRQ | 9589 | | | |
| UQCRFS1 | 21,609 | | | |
| UQCRFS1 transit peptide | 7,955 | | | |
| MTCYB | 42,591 | | | |
| CyC1 | 27,987 | | | |
| Complex III (Partial monomer)<br>CyB CyC UQCRC2 UQCRFS1 UQCRB UQCRQ UQCR10 | 168,970 | 168,580±50 | 390 | 0.23 |
| 2xComplex III (Partial monomer) | 337,940 | 338,615±12 | 675<br>heme | 0.199 |
| Subunit/Complex<br>Complex IV | Expected mass (Da) | Measured mass (Da) | Mass difference (Da) | Mass difference (%) |
| Cox1 | 57,032 | | | |
| Cox2 | 26,021 | | | |

| | | | | |
|---|---|---|---|---|
| Cox3 | 29,933 | | | |
| Cox4 Isoform 1 | 17,152 | | | |
| Cox5A | 12,433 | | | |
| Cox5B | 10,670 | | | |
| Cox6A1 | 9,538 | | | |
| Cox6B1 | 10,025 | | | |
| Cox6C | 8,478 | | | |
| Cox7A2 | 6,609 | | | |
| Cox7B | 6,357 | | | |
| Cox7C | 5,441 | | | |
| Cox8B | 4,961 | | | |
| Heme a | 853 | | | |
| Heme a3 | 859 | | | |
| Cardiolipin (CDL)* | 1448 | | | |
| Phosphatydilethanolamine (PE)* | 760 | | | |
| Complex IV monomer | 208,299 | 208,191±55 | 108 | 0.04 |
| Subunit/Complex<br>Complex V | Expected mass (Da) | Measured mass (Da) | Mass difference (Da) | Mass difference (%) |
| α** | 55,263 | 55,271±0.5 | 8 | 0.0144 |
| β** | 51,563 | 51,754±0.5 | 191 | 0.3 |
| γ** | 30,256 | 30,143±4 | 113 | 0.3 |
| δ** | 15,065 | 15,064±2 | 1 | 0.066 |
| ε** | 5,793 | 5,652±1 | 141 | 2.4 |
| a** | 24,788 | 24,813±4 | 25 | 0.1 |
| b** | 24,669 | 24,691±1 | 22 | 0.089 |
| c** | 7,608 | 7,650±1 | 42 | 0.55 |
| d** | 18,692 | 18,602±3 | 90 | 0.48 |
| e** | 8,321 | 8190±2 | 131 | 1.5 |
| f** | 10,297 | 10,206±2 | 91 | 0.8 |
| g** | 11,417 | 11,326±2 | 91 | 0.7 |
| A6L** | 7,973 | 7,963±1 | 10 | 0.1 |
| F6** | 8,958 | 8,957±2 | 1 | 0.01 |

| | | | | |
|---|---|---|---|---|
| 6.8PL** | 6,834 | 6,834±1 | 0 | 0 |
| DAPIT** | 6,453 | 6,303±1 | 150 | 2.32 |
| OSCP** | 20,930 | 20,929±4 | 1 | 0.004 |
| Holocomplex (8 c, 3 α, 3 β, 1copy of all the rest) | 581,948 | 581,046±62 | | 0.15 |
| Subunit/Complex<br>Complex I | Expected mass (Da) | Measured mass (Da) | Mass difference (Da) | Mass difference (%) |
| NDUFS7 | 20,077 | | | |
| NDUFS8 | 20,195 | | | |
| NDUFV2 | 23,814 | | | |
| NDUFS3 | 26,413 | 26,612 | | |
| NDUFS2 | 49,146 | | | |
| NDUFV1 | 48,499 | | | |
| NDUFS1 | 76,960 | | | |
| NU1M | 35,670 | | | |
| NU2M | 39,254 | | | |
| NU3M | 13,054 | | | |
| NU4M | 52,099 | | | |
| NU4LM | 10,797 | | | |
| NU5M | 68,286 | | | |
| NU6M | 19,078 | | | |
| NDUFS6 | 10,535 | | | |
| NDUFA12 | 17,090 | | | |
| NDUFS4 | 15,337 | | | |
| NDUFA9 | 39,115 | | | |
| NDUFAB1 | 10,109 | | | |
| NDUFA2 | 10,948 | | | |
| NDUFA1 | 8,105 | | | |
| NDUFB3 | 11,009 | | | |
| NDUFA5 | 13,184 | | | |
| NDUFA6 | 14,922 | | | |
| NDUFA11 | 14,626 | | | |
| NDUFB11 | 2,325 | | | |
| NDUFS5 | 12,536 | | | |
| NDUFB4 | 15,053 | | | |
| NDUFA13 | 16,542 | | | |
| NDUFB7 | 16,266 | | | |
| NDUFA8 | 19,959 | | | |
| NDUFB9 | 21,657 | | | |

| | | | | |
|---|---|---|---|---|
| NDUFB10 | 20,956 | | | |
| NDUFB8 | 2,537 | | | |
| NDUFC2 | 14,096 | | | |
| NDUFB2 | 8,493 | | | |
| NDUFA7 | 12,545 | | | |
| NDUFA8 | 9,217 | | | |
| NDUFA4 | 9,324 | | | |
| NDUFB5 | 16,726 | | | |
| NDUFB1 | 6,966 | | | |
| NDUFC1 | 5,828 | | | |
| NDUFA10 | 36,692 | | | |
| NDUFA4L2 | 9,984 | | | |
| NDUFV3 | 8,437 | | | |
| BDUFB6 | 15,392 | | | |
| Complex I ΔNDUFV1 ΔNDUFS1 ΔNDUFA6 (42/45 subunit, each present in one copy) | 809,202 | 809,101±57 | 101 | 0.012 |
| Complex I ΔNDUFV1 ΔNDUFS1 ΔNDUFA6 ΔNDUFS3 (41/45 subunits) | 782,789 | 782478±27 | 311 | 0.039 |

*Lipid identities from (*42*).

**Subunit masses measured by a monolithic column construct.

***Measurement from native MS.


41. L. A. Baker *et al.*, Magic-angle-spinning solid-state NMR of membrane proteins. *Methods Enzymol* **557**, 307-328 (2015).
42. S. Yoshikawa, K. Muramoto, K. Shinzawa-Itoh, M. Mochizuki, Structural studies on bovine heart cytochrome c oxidase. *Biochim Biophys Acta* **1817**, 579-589 (2012).
43. R. J. Rose, E. Damoc, E. Denisov, A. Makarov, A. J. Heck, High-sensitivity Orbitrap mass analysis of intact macromolecular assemblies. *Nat Methods* **9**, 1084-1086 (2012).
44. J. Gault *et al.*, High-resolution mass spectrometry of small molecules bound to membrane proteins. *Nat Methods* **13**, 333-336 (2016).
45. S. S. Bird, V. R. Marur, M. J. Sniatynski, H. K. Greenberg, B. S. Kristal, Lipidomics profiling by high-resolution LC-MS and high-energy collisional dissociation fragmentation: focus on characterization of mitochondrial cardiolipins and monolysocardiolipins. *Analytical chemistry* **83**, 940-949 (2011).
46. C. Bechara *et al.*, A subset of annular lipids is linked to the flippase activity of an ABC transporter. *Nat Chem* **7**, 255-262 (2015).
47. A. Shevchenko, H. Tomas, J. Havlis, J. V. Olsen, M. Mann, In-gel digestion for mass spectrometric characterization of proteins and proteomes. *Nat Protoc* **1**, 2856-2860 (2006).

48. D. N. Mastronarde, Automated electron microscope tomography using robust prediction of specimen movements. *J Struct Biol* **152**, 36-51 (2005).
49. P. C. Hsu *et al.*, CHARMM-GUI Martini Maker for modeling and simulation of complex bacterial membranes with lipopolysaccharides. *J Comput Chem* **38**, 2354-2363 (2017).
50. K. H. Kim *et al.*, Structural characterization of Escherichia coli BamE, a lipoprotein component of the beta-barrel assembly machinery complex. *Biochemistry* **50**, 1081-1090 (2011).
51. S. K. Fegan, M. Thachuk, Suitability of the MARTINI Force Field for Use with Gas-Phase Protein Complexes. *J Chem Theory Comput* **8**, 1304-1313 (2012).
52. G. Bussi, D. Donadio, M. Parrinello, Canonical sampling through velocity rescaling. *J Chem Phys* **126**, 014101 (2007).
53. M. Parinello, A. Rahman, Polymorphic transitions in single crystals: A new molecular dynamics method. *J Appl Phys* **52**, 7182-7190 (1981).
54. B. Hess, C. Kutzner, D. van der Spoel, E. Lindahl, GROMACS 4: Algorithms for Highly Efficient, Load-Balanced, and Scalable Molecular Simulation. *J Chem Theory Comput* **4**, 435-447 (2008).
55. W. Humphrey, A. Dalke, K. Schulten, VMD: visual molecular dynamics. *J Mol Graph* **14**, 33-38, 27-38 (1996).
56. T. Taverner *et al.*, Subunit architecture of intact protein complexes from mass spectrometry and homology modeling. *Accounts of chemical research* **41**, 617-627 (2008).
57. M. T. Marty *et al.*, Bayesian deconvolution of mass and ion mobility spectra: from binary interactions to polydisperse ensembles. *Analytical chemistry* **87**, 4370-4376 (2015).
58. N. Morgner, F. Montenegro, N. P. Barrera, C. V. Robinson, Mass spectrometry--from peripheral proteins to membrane motors. *J Mol Biol* **423**, 1-13 (2012).
59. M. Zhou *et al.*, Mass spectrometry of intact V-type ATPases reveals bound lipids and the effects of nucleotide binding. *Science* **334**, 380-385 (2011).